Oxidation and Mass Transfer in Heavy Liquid Metal Loops

H. Steiner, J. Konys

Institut für Materialforschung
Programm Nukleare Sicherheitsforschung

April 2006

Oxidation and mass transfer in heavy liquid metal loops

H. Steiner, J. Konys

Institut für Materialforschung

Programm Nukleare Sicherheitsforschung

Oxidation and mass transfer in heavy liquid metal loops

Abstract

A simple method has been devised to calculate the mass transfer in liquid metal loops. It is based on the use of mass transfer coefficients which determine the mass flux from the wall into the fluid. These coefficients depend on a dimensionless characteristic thermo-hydraulic number, namely the Sherwood number, which itself depends under forced convection flow conditions on the Reynolds number and the Schmidt number. This is supplemented by the application of the mass conservation law, which allows the calculation of the conditions in the bulk of the fluid. The newly developed kinetic model for mass transfer under forced convection flow conditions has been implemented in the computer code MATLIM.

The formation of protective oxide scales on stainless steel components is of prime importance for lead and lead-bismuth loops. As the propensity for mechanical effects like delamination and spalling increases with the thickness of the oxide scale, it is indispensable to have a clear understanding of the physical effects contributing to their growth. Thus, the importance of dissolution effects on oxide scales must be investigated and quantified, especially the dependence on the oxygen content in the liquid metal. This determines also the mass transfer from the hot leg to the cold leg in these loops. At higher temperatures dissolution attack of stainless steel specimens has been observed in some cases for oxygen contents in lead-bismuth alloy normally sufficient for oxide scale formation.

Dissolution effects on pre-existing oxide or other protective scales are also of great importance for lead-lithium loops. These loops are operated at very low oxygen contents in order to avoid the formation of Li_2O. With the loss of protective scales heavy dissolution attack of stainless steel components commences.

Oxidation und Massetransport in Schwermetall-Kreisläufen

Zusammenfassung

Um den Massetransport in Schwermetall-Kreisläufen zu berechnen, wurde ein einfaches Verfahren entwickelt. Es beruht auf der Benutzung von experimentellen Korrelationen für den Masseübertragungs-Koeffizienten. Diese sind bestimmt durch die charakteristische, dimensionslose thermohydraulische Kennzahl, die so genannte Sherwood Zahl, die ihrerseits bei Zwangsumlauf von zwei weiteren dimensionslosen Kennzahlen abhängt, nämlich der Reynolds Zahl und der Schmidt Zahl. Dies wird ergänzt durch die Anwendung einer Integralgleichung für die Masseerhaltung. Dieses neu entwickelte kinetische Modell wurde in den Computercode MATLIM eingebaut.

Die Bildung von schützenden Oxidschichten auf Bauteilen aus Edelstahl ist für Blei-Wismut Kreisläufe von eminenter Bedeutung. Da die Wahrscheinlichkeit für das Auftreten von mechanischen Effekten wie Ablösen und/oder Abplatzen der Oxidschicht aller Voraussicht nach mit deren Dicke zunimmt, ist ein klares Verständnis der beitragenden physikalischen Effekte unbedingt erforderlich. In diesem Zusammenhang müssen Ablösevorgänge untersucht und möglichst quantitativ beschrieben werden, besonders als Funktion des Sauerstoffgehalts im Flüssigmetall. Dies bestimmt dann auch den Massetransport vom heißen in den kalten Teil des Kreislaufs. Bei höheren Temperaturen wurde auch direkter Lösungsangriff von metallischen Werkstoffen beobachtet, und zwar bei Sauerstoffkonzentrationen im Blei-Wismut, die normalerweise für die Bildung von Oxidschichten ausreichend waren.

Ablöseeffekte an voroxidierten oder anderweitig beschichteten Stahlbauteilen sind auch für Blei-Lithium Kreisläufen von großer Bedeutung. Diese Kreisläufe werden in der Regel bei niedrigem Sauerstoffgehalt betrieben, um die Bildung von Li_2O zu vermeiden. Nach dem Verlust der schützenden Passivierungsschicht ist in diesen Kreisläufen mit starkem Lösungsangriff zu rechnen.

CONTENT   Page

1. Introduction

Liquid metal alloys have various applications in technical systems the most famous example is the sodium cooled Fast Breeder Reactor. Recently, Lead-Bismuth Eutectic (LBE) is foreseen as coolant and target in accelerator driven nuclear systems (ADS). Also, Pb-Li alloys are investigated as a coolant and breeding medium in future fusion reactors. One major problem in non-isothermal liquid metal systems lies in the corrosion of their structural components, consisting mainly of martensitic and austenitic stainless steels.

The formation of oxide scales on the structural components is considered as a viable measure in limiting the dissolution rates in the hot parts of the system, as the solubility of the oxides is in general much smaller than that of the metal alloys. Oxide scales might not be stable as for example in Pb-17Li alloy, but there may also be a problem in LBE loops at low oxygen concentrations. Hence, the prediction of the oxide scale evolution is of great importance. Also precipitation of oxides at cooler parts of the system can have consequences as there may be clogging and plugging of components having small cross sections. This may also affect maintenance and repair of the system as in an accelerator driven system there will be activation of steel components and there will be a transport of activated material from the hot leg to the cold leg.

The locations of dissolution and precipitation are mainly determined by the temperature dependence of the solubility of the oxides or of the metal alloys if no oxide scale is present. This means that we have dissolution in the hot leg of the system and precipitation in the cold leg, irrespective of the nature of the dissolution process, whether it is exothermic or endothermic.

We have developed a simple kinetic model, which calculates the mass transfer and the geometrical changes of structural components in liquid metal loops. This model was implemented in the computer code MATLIM. In two foregoing papers [1, 2] we have reported on an early version of this code for uni-modular heavy liquid metal loops. In this note we deal with the extension to multi-modular loops. The computer code can be applied to any sort of liquid metal loop, one has only to implement the relevant material data correlations. But in this note we will concentrate on lead-bismuth loops. These loops are operated under oxygen control that means at a level of oxygen concentration in the liquid metal sufficient for oxide scale formation on stainless steel components. We are mainly interested in two aspects, namely oxide scale formation and dissolution effects on oxide scales.

The newly developed model can be applied for any heavy liquid metal loop. In this report we are dealing with lead-bismuth and lead-lithium loops. Pb-Li loops are operated at very low oxygen contents in order to avoid formation of Li_2O. Thus, no oxide scales are formed on steel components in such loops. But questions of dissolution effects on oxide scales or other protective scales can arise. Pb-Bi loops are operated under oxygen control in such a way that oxide scale formation is assured. We think that, depending on the oxygen content in the liquid metal, on the temperature, and on the flow rate, dissolution effects on the oxide scales can become important and must therefore be investigated.

2. Convective diffusion

In general, one has forced convection flow conditions in liquid metal loops, either laminar or turbulent flow. If one wants to calculate the transport of ions, atoms, or molecules present in the liquid metal in a certain concentration c_i (with i denoting the solute), one can solve the convective diffusion equation (cp. ref. [3]):

$$\frac{\partial c_i}{\partial t} + (\vec{\upsilon}\nabla)c_i = \nabla(D_i \nabla c_i) \tag{1}$$

$\vec{\upsilon}$ is the velocity of the liquid metal and D_i the diffusivity of solute i in the liquid metal.

The convective diffusion equation is given in its most general form, assuming that the concentration can depend on the axial position x in the loop and on transversal coordinates and that there can be a transient phase.

Such a procedure has been adopted by Zhang and Li, which have published a series of papers [3-6]. But one can also take a different route for the solution of the problem. Namely, one can take profit of the principles of convective mass transfer, which stipulate that under forced convection flow conditions the mass flux is determined by a dimensionless characteristic flow parameter, the so-called Sherwood number; and we can take profit (if needed) of the analogy between heat and mass transfer.

Thus, the mass flux of the solute i from the channel wall into the bulk of the fluid is given by the following equation (cp. ref. [7]):

$$j_i = K_i^{fl} \cdot (c_i^{w} - c_i^{b}) \tag{2}$$

K_i^{fl} is the mass transfer coefficient for the solute i *from the wall into the fluid*, c_i^{w} the concentration of the solute *i* at the wall and c_i^{b} is the concentration in the bulk of the fluid. If c_i^{w} is greater than c_i^{b} there is dissolution otherwise there is precipitation. In eq. (2) it is assumed that the solute i is precipitated at the wall of the channel. There are indications from the PICOLO loop that there can also be precipitation of metallic particles in the cold leg. This phenomenon is not yet included in the model.

The direction of the mass flux depends on the ratio of the two concentration values. If c_i^{w} is higher than c_i^{b} then the mass flux is directed from the wall into the fluid; if c_i^{w} is smaller than c_i^{b} then the mass flux is directed from the fluid to the wall.

In the following we make implicitly use of the fact that the solutions of the thermo hydraulic equations depend on characteristic non-dimensional quantities, which is finally a consequence of Buckingham's Π-theorem [8].

The mass transfer coefficient in the fluid K_i^{fl} is determined by the Sherwood number Sh in the following way:

$$K_i^{fl} = \frac{D_i}{d_{hyd}} \cdot Sh \qquad (3)$$

d_{hyd} is the hydraulic diameter of the flow channel.

The mass transfer coefficient in the fluid can be used to obtain an estimate for the diffusion boundary layer thickness in the liquid metal:

$$K_i^{fl} = \frac{D_i}{\delta_{diff,i}^{fl}} \qquad (4)$$

Bringing the convective diffusion equation (1) into a non-dimensional form, one can show that under forced convection flow conditions its solutions depend on the Reynolds number Re and on the Schmidt number Sc. Thus, the Sherwood number Sh, which is the characteristic number for the non-dimensional mass flux, must also depend on the Reynolds number Re and on the Schmidt number Sc. Therefore we have the following functional relationship:

$$Sh = a \cdot Re^\alpha \cdot Sc^\beta \qquad (5)$$

The parameters *a*, α, and β depend on the flow regime and must be determined experimentally.

The Reynolds number and the Schmidt number are defined as:

$$Re = \frac{u_{fl} \cdot d_{hyd}}{\upsilon_{fl}} \qquad Sc = \frac{\upsilon_{fl}}{D_i} \qquad (6)$$

υ_{fl} is the kinematic viscosity of the fluid and u_{fl} the flow velocity.

It remains to calculate the solute concentration in the bulk of the fluid c_i^b along the whole loop. This is done with the help of the mass conservation law. In this way we have derived the following differential equation:

$$\frac{\partial c_i^b(t,x)}{\partial t} + u_{fl} \cdot \frac{\partial c_i^b(t,x)}{\partial x} = \frac{U_{ch}}{A_{ch}} \cdot j_i(t,x) \qquad (7)$$

U_{ch} is the circumference of the flow channel, A_{ch} the cross section of the flow channel

The axial position x in the loop is to be understood as a length of flow path, as the different axial sections of the loop are added in a scalar way irrespective of their orientation in space.

There we have assumed that the bulk concentration does not depend on transverse coordinates, as the concentration c_i^b in the liquid metal is practically uniform, with appreciable concentration differences appearing only in a very thin layer at the wall. This thin layer was neglected in the derivation of eq. (7).

2.1 Fanning friction factor

The Fanning friction factor λ depends only on the Reynolds number. Different correlations have to be used for the different flow regimes [9].

$$\text{For} \quad \text{Re} \leq 2300 \quad \lambda = \frac{16}{\text{Re}} \tag{8}$$

$$\text{For} \quad \text{Re} \leq 2300 \quad \lambda = \frac{16}{\text{Re}} \tag{8}$$

$$\text{For} \quad 2300 \leq \text{Re} \leq 2 \cdot 10^4 \quad \lambda = \frac{0.079}{\text{Re}^{0.25}} \tag{9}$$

$$\text{For} \quad \text{Re} \geq 2 \cdot 10^4 \quad \lambda = \frac{0.046}{\text{Re}^{0.2}} \tag{10}$$

2.2   Shear stresses at the wall

The shear stress at the wall can be calculated with the help of the following formula [9]:

$$\tau = \rho_{fl} \cdot u_{fl}^2 \cdot f_W / 8 \qquad (11)$$

f_W = Weisbach friction factor ($f_W = 4\lambda$)

A Reynolds number of $2.9 \cdot 10^5$ leads to a value of 0.015 for the Weisbach friction factor f_W and for a flow velocity of 200 cm/s one obtains a value of 780 dyn/cm^2 that is $0.78 \cdot 10^{-4}$ MPa.

3.   Dissolution and precipitation rates

We have now all the necessary elements for the calculation of the dissolution and the precipitation rates, one of the main aims of this work. We are mainly concerned with stainless steel components and in the foregoing we will derive formulas relevant for this kind of material. If we have an oxide scale consisting of magnetite the dissolution and precipitation rates are given as:

$$b_{ox} = -j_{Fe} \cdot \frac{3 \cdot M_{Fe} + 4 \cdot M_O}{3 \cdot M_{Fe}} / \rho_{ox} \qquad (12)$$

j_{Fe} is the iron flux, M_i the atomic weight of the species i and ρ_{ox} the specific density of the magnetite.

If we have an iron-chromium spinel, the ratio of the atomic weights in eq. (13) has to be modified accordingly. We have adopted the convention that in case of dissolution the rate b^{ox} is negative and in case of precipitation positive.

If there is no oxide scale present, the dissolution and precipitation rates depend a bit on the behavior of all the alloying components. If f_{Fe} measures the mass fraction of all the alloying elements of the cladding dissolved or precipitated which can be attributed to iron, we get:

- 11 -

$$b_{me} = -j_{Fe} \cdot \frac{1}{\rho_{ss} \cdot f_{Fe}} \tag{13}$$

ρ_{ss} is specific density of stainless steel.

It should be noted that in both cases the calculated iron flux which appears in eqs. (12) and (13) is very different, as the solubility can differ by order of magnitudes.

4. Evolution of the oxide scale and of the channel wall inner radius

If the concentration of oxygen in the liquid metal is above a certain limiting value, oxide scales are formed on the stainless steel components. We assume that in the absence of dissolution the increase of the oxide scale can be described by some function $r(T,c_O)$ for the oxidation rate, then we can establish the following balance equation for the oxide scale:

$$\frac{d\delta_{ox}(t)}{dt} = r(T,c_O) + b_{ox} \tag{14}$$

c_O: oxygen concentration in the liquid metal.

A similar equation has originally been used by Tedmon [10] for high-temperature oxidation of Cr_2O_3 with simultaneous volatilization.

If the liquid metal loop is operated at a very low oxygen concentration as is the case for Pb-17Li, no new oxide is formed and we have:

$$\frac{d\delta_{ox}(t)}{dt} = b_{ox} \tag{15}$$

In the high temperature region we have dissolution and b_{ox} is negative and the oxide scale is gradually dissolved at a constant rate b_{ox}. The so-called incubation phase is terminated at a certain axial location x, when the dissolution of the oxide scale is completed.

In a time increment Δt the inner channel wall radius will change by:

$$\Delta r_i^{ch} = -\frac{b_{ox}}{\Phi} \cdot \Delta t - \frac{\delta_{ox}}{\Phi} \tag{16}$$

Φ is the Pilling-Bedworth ratio.

If no oxide scale is present on the inner clad wall, we have in the dissolution and in the precipitation regime the following equation:

$$\Delta r_i^{ch} = -b_{me} \cdot \Delta t \tag{17}$$

In case the oxygen concentration in the liquid metal is below the critical value for oxide scale formation, no oxide is precipitated and the rate b_{me} is to be applied to calculate the evolution of the inner channel wall in the precipitation regime.

5.   Boundary conditions

We have also to fix the boundary conditions. In a closed loop we have the following periodic boundary condition:

$$c_i^b(t,0) = c_i^b(t,L) \tag{18}$$

L is the total length of the loop.

In a pipe flow situation we would have in most cases the following condition at the inlet:

$$c_i^b(t,0) = c_i^0(t) \tag{19}$$

x = 0: axial position of the inlet.

If there is a magnetic trap at some axial location $x_{m.tr.}$, which is able to remove the solute i quantitatively, we would also have:

$$c_i^b(t,x_{m.tr.}) = C_{Fe}^{s,m.tr.} \tag{20}$$

This extreme condition will in reality not be reached. The efficiency of a magnetic trap will depend on a lot of parameters, especially on the strength of the magnetic field

and on the distribution of iron or other metallic particles. These problems are beyond the possibilities of the present version of MATLIM.

The value which we have to take for c_i^w depends on the nature of the interface. If the solute results from an interface reaction with rate constant k_s we have a two step mechanism and the overall mass transfer coefficient K_t is given by [11]:

$$K_t = \frac{k_s \cdot K_i^{fl}}{k_s + K_i^{fl}} \qquad (21)$$

When $k_s \gg K_i$ then $K_t \to K_i^{fl}$. We have also assumed that there is no diffusion surface layer, which the solute i must pass. Otherwise, the overall mass transfer coefficient is given by:

$$K_t = \frac{K_i^{fl} \cdot D_i^{s.l.}/\delta_s}{K_i^{fl} + D_i^{s.l.}/\delta_s} \qquad (22)$$

$D_i^{s.l.}$ is the diffusion coefficient of the species i in the surface layer and δ_s the thickness of the surface layer.

Using the overall mass transfer coefficient we have the following equation:

$$j_i = K_t \cdot (c_i^w - c_i^b) \qquad (23)$$

In general, diffusion is a slow process compared to chemical reactions. Therefore we assume that the rate constant of the interface reactions, is much higher than the mass transfer coefficient in the liquid metal. Thus, we have:

$$K_t = K_{Fe}^{fl} \qquad (24)$$

As concerns the iron concentration at the wall, which we need as a boundary condition, we have to consider different situations. If there is an oxide scale present on the metallic component we should use the iron solubility relevant for the oxide phase present at the surface:

$$c_{Fe}^{w} = c_{Fe}^{s} \qquad (25)$$

But if there is no oxide scale present and we have dissolution of the metallic substrate, we have two possibilities. We can either use the iron solubility for the metallic alloy in the same way as in eq. (25), or as there are other alloying elements dissolved in the liquid metal, we can use the following boundary condition:

$$c_{Fe}^{w} = a_{Fe} \cdot c_{Fe}^{s} \qquad (26)$$

a_{Fe} = iron activity in the liquid metal

This view has not yet been expressed in the literature. In order to make use of this boundary condition we need, of course, values for the iron activity for the stainless steels used in the loops. In ref. [12] correlations for the thermodynamic activities of the alloying elements in AISI 316 are reported. For iron the following correlation was given:

$$\log a_{Fe}(T) = 0.179 - 248.54/T \qquad (27)$$

T in K

For T = 823 K we obtain a_{Fe} = 0.755

In ref. [13] are given thermodynamic activities of solid alloys of chromium with nickel and iron. For a Cr-content of 0.1 we would obtain a_{Fe} = 0.9.

The boundary condition (25) is generally used in the literature (see for example refs. [3 and 7]). In case of metallic surfaces, as in the PICOLO loop, we assume also that there is no diffusion layer at the surface of the wall. This condition can be removed, if in the future we can get experimental evidence for such surface layers. According to ref. [14] porous ferritic layer are observed on the surface of austenitic steels which are characterized by a depletion of nickel, manganese and chromium. Ferritic and martensitic steels, on the other hand show no such surface layer [14]. The presence of porous surface layers could eventually be not observed by metallography, as they may be very friable. They would in any case necessitate the use of an iron diffusivity value in the liquid metal distinctly lower than in reality, if they are not included in the model.

6. Correlations for the mass transfer coefficient

The newly developed model has been incorporated in the computer code MATLIM, where the relevant differential equations are solved with the help of finite difference techniques by dividing the whole loop into a certain number of axial meshes. In the actual version of the code a value of 1000 axial meshes is used. But this value can easily be increased if there is a need. In this way multi-modular loops can easily be treated, as specific values for the relevant parameters can be assigned for each axial mesh

There are mainly three different types of physical properties and parameters, which determine material behavior in a liquid metal system. The first group concerns the thermo-hydraulic data of the system like the flow velocity and the hydraulic diameter but also the temperature distribution along the system. The second group concerns material data like viscosity of the liquid metal, diffusivity and solubility of the solutes. The third group encompasses properties of the wall materials itself like oxidation rates. The dependence on the thermo-hydraulic parameters is evident from eqs. (28) - (30) and will be discussed in the following for turbulent and laminar flow conditions.

There are a number of experimental correlations for the mass transfer coefficient obtained under fully developed turbulent pipe flow. Our main assumption is that they can also be applied for liquid metal loops in case they obey the general functional relationship of eq. (5) (principle of similarity for forced convection flow). An additional requirement, which must be fulfilled, is that the experimental range of the Reynolds number and the Schmidt number should correspond to that relevant for heavy liquid metal loops. Otherwise the errors of extrapolation could become rather large.

Three of these correlations were investigated and discussed in ref. [7]. These are the correlation of Berger and Hau [15], that of Silverman [16], and that of Harriott and Hamilton [17]. The range of validity for the Berger and Hau correlation, for example, is given in ref. [7] as follows:

$$8 \cdot 10^3 \leq \mathrm{Re} \leq 2 \cdot 10^5, \ 1000 \leq \mathrm{Sc} \leq 6000 \tag{24}$$

It was obtained from the ferricyanide/ferrocyanide reaction on pieces of nickel tube with a polished inner surface ensuring a roughness of about 1 μm.

We reproduce these correlations of mass transfer for turbulent pipe flow conditions as given in ref. [7]:

$$K_{B-H} = 0.0165 \cdot u_{fl}^{0.86} \cdot D_{Fe}^{0.670} / (d_{hyd}^{0.14} \cdot v_{fl}^{0.530} \tag{28}$$

$$K_{Silv} = 0.0177 \cdot u_{fl}^{0.875} \cdot D_{Fe}^{0.704} / (d_{hyd}^{0.125} \cdot v_{fl}^{0.567}) \tag{29}$$

$$K_{H-H} = 0.0096 \cdot u_{fl}^{0.913} \cdot D_{Fe}^{0.654} / (d_{hyd}^{0.087} \cdot \nu_{fl}^{0.567} \tag{30}$$

All these three correlations give similar values for the mass transfer coefficient. It is therefore sufficient for us to use only one of them, namely that of Silverman [16]:

In case of laminar flow we can make use of the analogy between heat and mass transfer. There is a lot of information on the heat transfer in pipe flow (laminar and turbulent, inlet flow or fully developed flow) in ref. [18], which can be applied to mass transfer by replacing the Nusselt number by the Sherwood number and the Prandtl number by the Schmidt number. The model incorporated in the code MATLIM is flexible enough, as in each axial mesh of the loop we can specify the value of the mass transfer coefficient. We are not going to discuss this in all details but only give here the Sherwood number for small values of the parameter $Re \cdot Sc \cdot d_{hyd} / x$ (x = axial distance from the inlet) [17]:

In case of a full circular cross-section [18]:

$$Sh_{la} = 3.66$$

In case of an annular cross-section [18]:   (31)

$$Sh_{la} = 3.66 + (4 - 0.102/(d_i / d_o + 0.02))(d_i / d_o)^{0.04}$$

d_i, d_o are inner, outer diameter of the flow channel.

There we have made use of the analogy between heat and mass transfer, that means replaced the Nusselt number by the Sherwood number.

We have applied the Nusselt number correlation given in [18] for fixed values of the wall temperature and not that for fixed values of the heat flux, as these values are to be transferred for a situation with fixed values for the concentration of the solutes at the wall. It should be noted that in case of fully developed laminar flow the mass transfer coefficient does not depend on the flow velocity and increases linearly with the iron diffusivity.

The flow in pipes is laminar up to a Reynolds number of 2300 and it becomes fully turbulent at a Reynolds number of 10000. In between we have a transition regime. In order to describe this transition regime we follow the procedure proposed in [18], which is based on a linear interpolation between the Nusselt numbers in the laminar and in the turbulent regime.

Defining the parameter γ as:

$$\gamma = \frac{\text{Re} - 2300}{10^4 - 2300} \tag{32}$$

we obtain the Sherwood number in the transition region as follows:

$$\text{Sh}_{tr} = (1 - \gamma) \cdot \text{Sh}_{la}(2300) + \gamma \cdot \text{Sh}_{turb}(10^4) \tag{33}$$

Sh_{turb} is the Sherwood number in the fully turbulent region.

7. Material data correlations

7.1 Solubility

Lead-bismuth alloys

Solubility data for liquid lead-bismuth eutectic (LBE) are given in ref. [3]. In case of the pure metal without an oxide scale the solubility of iron is accordingly:

$$c_{Fe}^{s}(T) = 10^{6.01 - 4380/T} \quad \text{in wppm} \tag{34}$$

In ref. [3] are also given solubility data for Ni, Cr and O as taken originally from [19]. It should be noted that the data for oxygen are different from that given in [20]. These are:

$$c_{O}^{s}(T) = 10^{5.2 - 3400/T} \tag{35}$$

$$c_{Ni}^{s}(T) = 10^{5.53 - 843/T} \tag{36}$$

$$c_{Cr}^{s}(T) = 10^{3.98 - 2280/T} \qquad (37)$$

As can be taken from Fig.1, Ni has by far the highest solubility in LBE. Therefore there can be Ni depletion effects in steels.

If there is Fe_3O_4 oxide scale present, the solubility is according to ref. [3]:

$$c_{Fe}^{s}(T, c_{O^{2-}}) = \frac{1}{c_o^{4/3}} 10^{11.35 - 12844/T} \qquad (38)$$

T = temperature in K c_o^- = oxygen concentration in LBE

As long as there is an oxide scale present on the metallic surface eq. (38) is to be applied, irrespective of the fact that below a limiting value of the oxygen concentration correlation (35) provides then lower values. This is different from the position taken in [3], where the intersection of eqs. (34) and (38) is determined and then the lower value is taken for the iron solubility. In case of precipitation the procedure proposed in ref. [3] can be applied. That means below a critical value of the oxygen content metal is deposited at the channel wall and otherwise oxide.

Depending on the temperature, the Cr content in the steel and the oxygen content in the liquid metal, the oxide scales of martensitic and austenitic steels can consist only of Fe/Cr spinel [21, 22]. We could not find solubility values for this substance in the literature, but following the line of thought explained in ref. [23] we were able to derive a correlation for $FeCr_2O_4$. For this substance data could be found in the literature (see for example ref. [24]). The main idea in ref. [23] is that Pb can reduce the oxide film, if the iron content in the liquid metal is too low. Thus the reduction of a magnetite scale is described in [23] by the following reaction equation:

$$\frac{1}{4} Fe_3O_4 + Pb = \frac{3}{4} Fe + PbO \qquad (39)$$

For the reduction of $FeCr_2O_4$ we can establish the following equation

$$\frac{1}{4} FeCr_2O_4 + Pb = \frac{1}{4} Fe + \frac{1}{2} Cr + PbO \qquad (40)$$
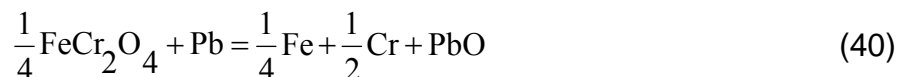
The equilibrium constant for this equation is given as:

$$\frac{a_{PbO} \cdot a_{Fe}^{1/4} \cdot a_{Cr}^{1/2}}{a_{Pb} \cdot a_{FeCr_2O_4}^{1/4}} = \exp(\frac{-\Delta G_{PbO}^f + 1/4 \cdot \Delta G_{FeCr_2O_4}}{R \cdot T}) \tag{41}$$

From the data given in ref. [24] we have derived the following correlations for the Gibbs' free energies:

$$\Delta G_{FeCr_2O_4}^f = -1455.4 + 0.334 \cdot T \tag{42}$$

$$\Delta G_{PbO}^f = -218.1 + 0.099 \cdot T \tag{43}$$

ΔG^f (in kJ/Mol) is the Gibbs' energy of formation from the elements in their reference state

Using these correlations and the solubility data for O, Fe and Cr given in ref. [3] we can establish the following correlation for the combined Fe/Cr solubility over a $FeCr_2O_4$ film:

$$c_{Fe}^{1/4}(c_O, T) \cdot c_{Cr}^{1/2}(c_O, T) = \frac{1}{c_O} \cdot 10^{7.891 - 13246/T} \tag{44}$$

In the same way as we have done for a $FeCr_2O_4$ film we can also derive the Cr solubility over a Cr_2O_3 film in Pb-Bi alloys. The equilibrium constant for the reduction of the chromia by Pb is then given as:

$$\frac{a_{PbO} \cdot a_{Cr}^{2/3}}{a_{Pb} \cdot a_{Cr_2O_3}^{1/3}} = \exp(\frac{-\Delta G_{PbO}^f + 1/3 \cdot \Delta G_{Cr_2O_3}^f}{R \cdot T}) \tag{45}$$

The Gibbs' free energy of formation for Cr_2O_3 is given by:

- 20 -

$$\Delta G^f_{Cr_2O_3} = -1135.3 + 0.259 \cdot T \qquad (46)$$

Using eq. (43) and (46), we obtain for the Cr solubility over a Cr_2O_3 film the following correlation:

$$c_{Cr}(T,c_O) = \frac{1}{c_O^{3/2}} \cdot 10^{10.8 - 19936/T} \qquad (47)$$

All concentrations are in ppm.

For an oxygen content of 0.01 ppm and a temperature of 823 K we would obtain values for the Cr solubility in the order of 10^{-10} ppm, whereas we would obtain for the Fe solubility over magnetite a value of about 0.03 ppm. Thus, Cr_2O_3 should be practically insoluble in Pb-Bi alloys under such conditions. Even for oxygen contents as low as 10^{-6} ppm we would obtain values for the Cr solubility in the range of 10^{-4} ppm. We do not know of any test of steel specimens with chromia scales in lead-bismuth alloys, but such scales should be similar in behaviour to alumina scales. It is known that alumina scales are corrosion resistant in lead-bismuth alloys [25].

In case of $FeCr_2O_4$ we would obtain for the solubility of (Fe+Cr) values in the range of 10^{-9} ppm. Thus, the dissolution effect on $FeCr_2O_4$ scales would be much smaller than that for magnetite. For Fe/Cr spinel with lower Cr contents we would expect smaller values for the free energy of formation than for $FeCr_2O_4$ and therefore higher metal solubility. But we think that it will be still considerably smaller than that for magnetite.
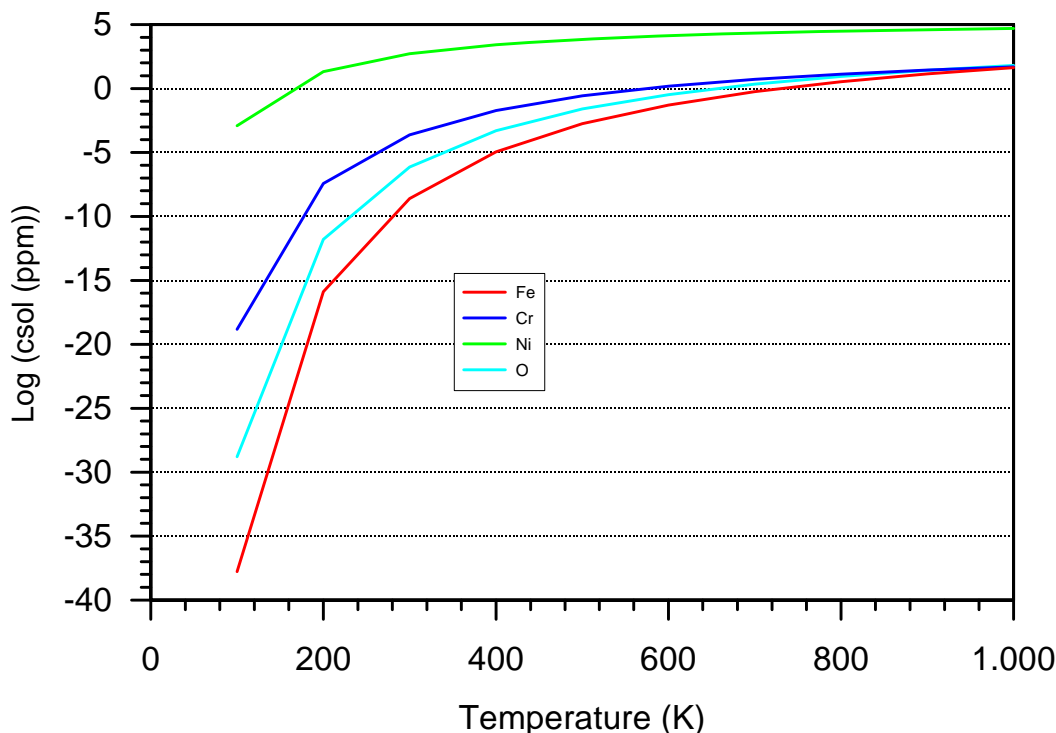

Fig.1 Solubility values of different metals and oxygen in LBE according to ref. [3]
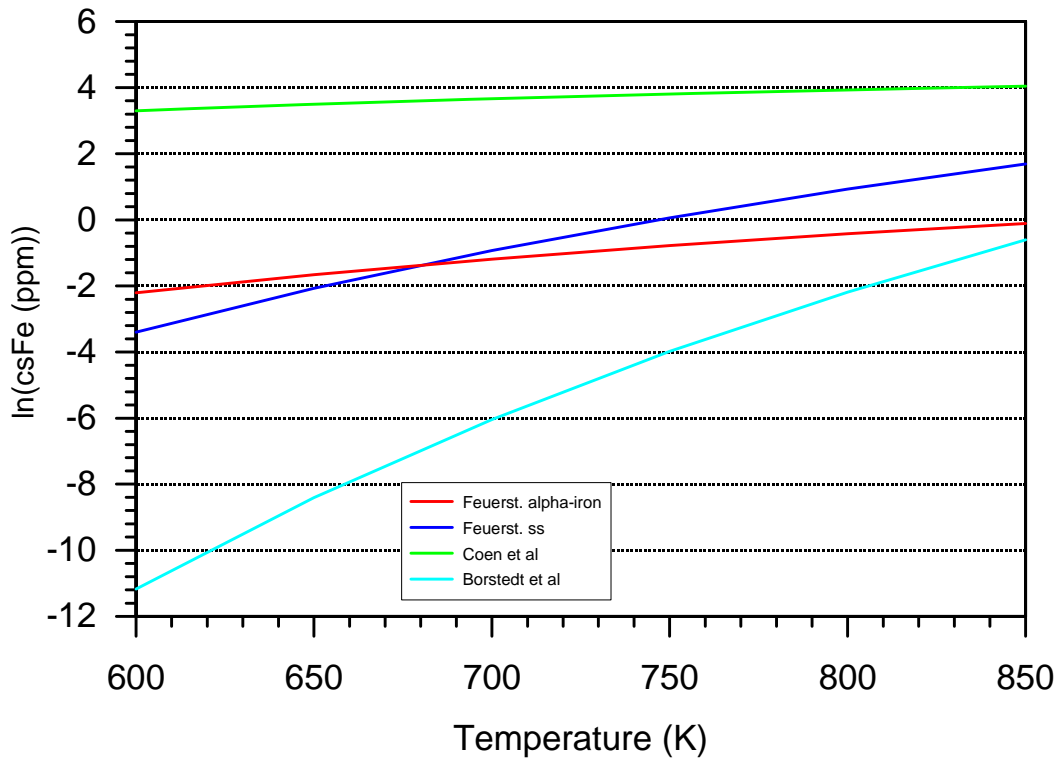
Fig.2 Iron solubility (c_{Fe}^s) in Pb-17Li versus temperature according to Feuerstein et al [31], Borgstedt et al [28], and Coen et al [26].

Pb-17Li

For Pb-17Li, the following correlation for the iron solubility was given in refs. [26, 27] and recommended in [7]:

$$c_{Fe}^s(T) = 10^{2.524 - 655.07/T}$$

(48)

The solubility data in ref. [28, 29] on the other hand would give values lower by about a factor of 1000:

$$c_{Fe}^s(T) = 10^{10.733 - 9345/T}$$

(49)

Coen et al [26] determined their correlation of the iron solubility by performing immersion tests determining the concentration of dissolved metal in the liquid alloy by atomic absorption spectroscopy. Borgstedt et al [28, 29] deduced the iron solubility

from dissolution tests in flowing Pb-17Li using a certain correlation for the mass transfer coefficient and certain values for the iron diffusivity (Sutherland-Einstein) and the Schmidt number. It should be noted that the solubility values of Borgstedt et al are close to that in unalloyed lead [29, 30].

The solubility of iron in Pb-17Li was also determined by Feuerstein et al [31] by dissolution tests in crucibles at 500 and 600°C. For tests done with α-iron the following correlation has been obtained:

$$c_{Fe}^{s}(T) = e^{4.94 - 4992/T}$$
(50)

This correlation gives a value of about 1 wppm at 600°C, considerably lower than the values given by the correlation (48). In ref. [31] were also compared the solubility correlations of iron of different authors and it was concluded that especially the values of Coen, Barker and Sample [26, 27] are too high.

Two data points for the iron solubility of stainless steels were also given in ref. [31] and from these two data points we have derived the following correlation:

$$c_{Fe}^{ss}(T) = 1.1016E6 \cdot e^{-10389/T}$$
(51)

At 600^{0}C this correlation yields a value of about 7.5 wppm, distinctly higher than that for

α-iron. A comparison of the different correlations for the iron solubility in Pb-17Li is to be found in Fig. 2.

If there is an oxide scale present on the metallic surface the respective solubility correlation relevant for the oxide is to be applied. There are correlations for the solubility of magnetite in Pb and LBE to be found in the literature [3], but not for any oxides in Pb-17Li.

In ref. [31] are given solubility correlations for a lot of other metals besides Fe from Al to Zr but unfortunately not for Cr and Ni.. We reproduce here the correlations for Mo and Ti:

$$c_{Mo}^{s}(T) = e^{10. - 9784/T}$$
(52)

$$c_{Ti}^{s}(T) = e^{21.3 - 13600/T}$$
(53)

Values for the solubility of Mn and Ni are also reported in ref. [14]. The respective correlations are as follows:

$$c_{Ni}^s(T) = 10^{4.832 - 981.2/T} \tag{54}$$

$$c_{Mn}^s(T) = 10^{6.732 - 2938/T} \tag{55}$$

The solubility of Cr was found to be very low and no sensible correlation could be established.

7.2 Diffusivity

The diffusivities of single-atom solutes in liquid metals are often calculated with the help of the Sutherland-Einstein equation [3, 7]:

$$D_i(T) = \frac{k \cdot T}{4 \cdot \pi \cdot \eta_{fl}(T) \cdot r_i} \tag{56}$$

η_{fl} is the dynamic viscosity of the fluid and r_i the atomic radius of the solute.

It should be noted that eq. (56) is satisfactorily accurate for large colloidal particles and even for very large molecules. Its accuracy becomes increasingly unsatisfactory as particle size decreases [9].Thus, its use for the calculation of the diffusivity of iron atoms in heavy liquid metals is at least doubtful. Also, iron may mainly exist in form of solvated metal clusters and not in the form of single atoms. Thus, one should use an effective cluster radius in eq. (56), which can be much larger than the "real" atomic radius.

With an atomic radius of $1.13 \cdot 10^{-7}$ mm for iron [7] and a dynamic viscosity of $1.25 \cdot 10^{-3}$ Pa·s for Pb-17Li at 500°C, one obtains for the diffusivity of iron in Pb-17Li the following value [7]:

$$D_{Fe}(550°C) = 6.4 \cdot 10^{-9} \cdot m^2/s \tag{57}$$

This theoretical value was compared to values of the diffusivity obtained from experiments with a rotating cylinder, which are smaller by a factor of about 10^{-5} [7].

The authors in ref. [31] have deduced the following correlation for the iron diffusivity in Pb-17Li from the dissolution rates in crucibles by applying a simple model for the dissolution rate:

$$D_{Fe}(T) = e^{-19.64 - 2844/T} \text{ in m}^2/\text{s} \tag{58}$$

For orientation we have plotted the iron diffusivity in Pb-17Li according to the two correlations in Fig. 3.

Experimental values of diffusion coefficients in various liquid metals have been collected in ref. [32]. They range in the order of 10^{-5} – 10^{-4} cm^2/s. For iron in liquid lead a value lower than $8.3 \cdot 10^{-6}$ cm^2/s is given for 643 K. No values have been provided for lead-bismuth alloys and for Pb-17Li only values for H and T. The experimental diffusion coefficients are frequently charged with a convectional overestimation, an underestimation is much less probable [32].
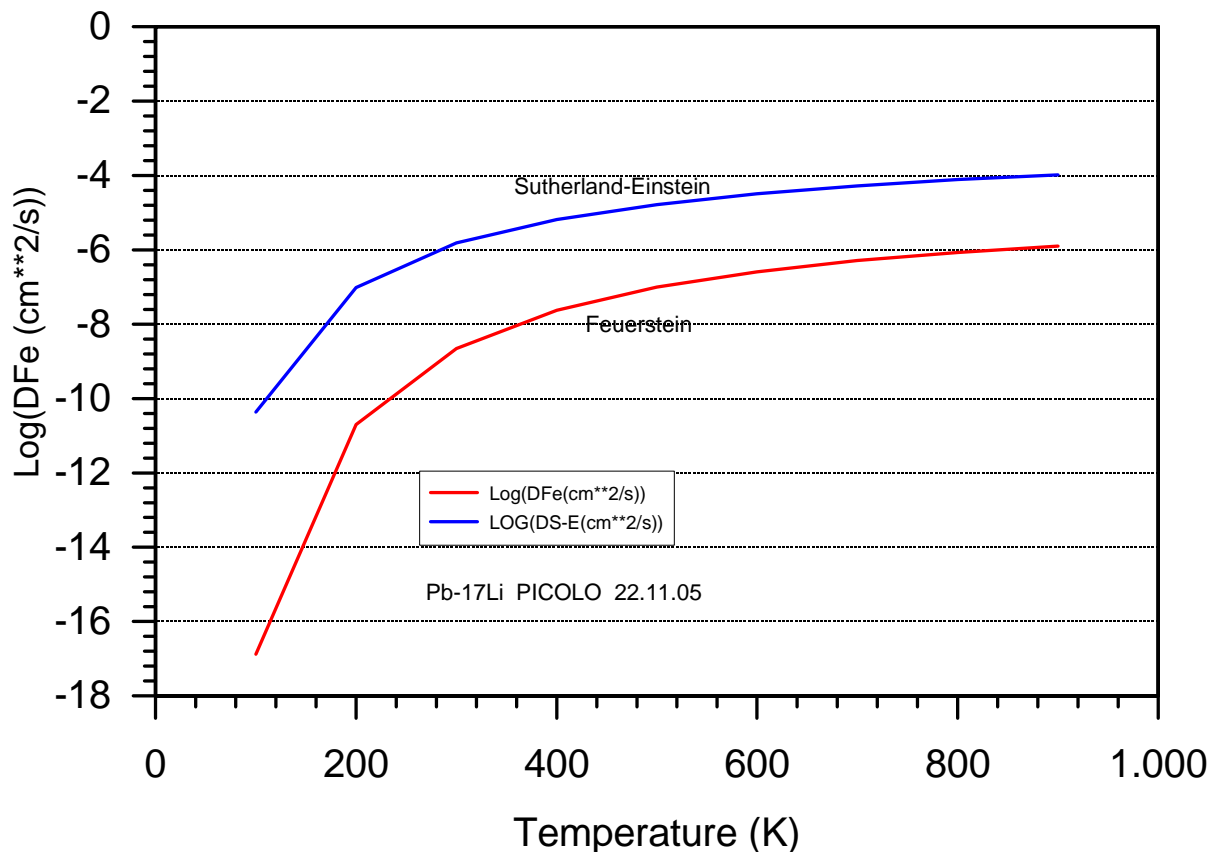

Fig.3 Iron diffusivity (D_{Fe}) in Pb-17Li according to the Sutherland-Einstein equation and according to Feuerstein et al [31]

7.3 Viscosity

7.4 Lead-bismuth alloys

For LBE the following correlation is recommended for the kinematic viscosity:

$$\nu_{fl}(T) = 0.49 \cdot 10^{-3} \cdot \exp(760.1/T) \quad \text{in cm}^2/\text{s} \tag{59}$$

7.5 Pb-17Li

For the kinematic viscosity of Pb-17Li the following correlation was given in [28]:

$$\nu_{fl}(T) = 1.9 \cdot 10^{-4} \cdot \exp(1406/T) \quad \text{in cm}^2/\text{s} \tag{60}$$

T = temperature in Kelvin

The kinematic viscosity of heavy liquid metals decreases slightly with increasing temperature. Increasing the temperature from 480 to 550 ^{0}C, would reduce the viscosity of Pb-17Li by about 15 %.

8. Technical information on MATLIM

8.1 Treatment of multi-modular loops

In general, heavy liquid metal loops will consist of a certain number of modules and of axial tubing sections, which can have different values for the hydraulic diameter and have different geometries (full or annular cross section for example). The CORRIDA loop is such a multi-modular loop. In order to deal with such situations, we make use of the fact that the fluid mass flow rate is constant along the loop. For the time being we do not foresee a bypass in some part of the loop. The constancy of the mass flow rate is expressed as follows:

$$A_i^{ch} \cdot \rho_i^{fl} \cdot u_i^{fl} = \text{const.} \qquad (61)$$

i= number of the axial section

In equation (xx) we have neglected the contribution of dissolved cladding components, as they comprise only a few wppm. To a first approximation we can also neglect the temperature dependence of the fluid density. The equation of continuity leads then to the following expression for the flow velocity in the different axial sections:

$$u_i^{fl} = u_{ref.}^{fl} \cdot \frac{A_{ref.}^{ch}}{A_i^{ch}} \qquad (62)$$

There we have made use of the fact that the nominal flow velocity in the loop is given for some reference axial section. For the PICOLO and CORRIDA loops it is the axial section with the test specimens the so-called test section), which is taken as reference.

The hydraulic diameter in each axial section is to be calculated with the help of the following formula, applicable also in case of non-circular cross sections:

$$d_{hyd,i} = \frac{4 \cdot A_i^{ch}}{U_i^{ch}} \qquad (63)$$

U_i^{ch} = wetted channel perimeter in the i th axial section

Most axial sections in the CORRIDA loop have full circular or annular cross sections. Thus, in order to calculate the three characteristic geometrical parameters U_i^{ch}, A_i^{ch} and $d_{hyd,i}$ it is sufficient to give the inner and outer radius of the flow channel as input. But also for components of a more complicated structure like the heat exchanger we can define equivalent values of the inner and outer radius of the flow channel in such a way that the three characteristic geometrical parameters are correct.

The heat exchanger in the CORRIDA loop consists of a pressure tube containing 151 internal flow tubes and 12 rods. Thus, in the heating mode the equivalent inner and outer radii of the flow channel are determined by the following equations:

$$r_o^{eq} + r_i^{eq} = r_i^{p.t.} + 151 \cdot r_o^{fl.t.} + 12 \cdot r_o^{rod} \tag{64}$$

$$(r_o^{eq})^2 - (r_i^{eq})^2 = (r_i^{p.t.})^2 - 151 \cdot (r_o^{fl.t.})^2 - 12 \cdot (r_o^{rod})^2 \tag{65}$$

In the cooling mode the equivalent radii are given by:

$$r_o^{eq} + r_i^{eq} = 151 \cdot r_i^{fl.t.} \tag{66}$$

$$(r_o^{eq})^2 - (r_i^{eq})^2 = 151 \cdot (r_i^{fl.t.})^2 \tag{67}$$

8.2   Numerical procedures

Finite difference techniques are applied for the solution of the differential equations and for the calculation of the integrals. In order to do this we have to divide each axial section of the loop into a certain number of equal-sized axial meshes. If $N_{ax,i}$ is the number of the axial meshes in the axial section i, then the axial length Δx of a mesh is given as:

$$\Delta x = \Delta l_i / N_{ax,i} \tag{68}$$

Δl_i = length of the i th axial sextion in the loop

The axial positions x_k of the boundaries of the k th axial mesh are then:

$$\begin{aligned} x_u &= (k-1) \cdot \Delta x \\ x_d &= k \cdot \Delta x \end{aligned} \tag{69}$$

x_u = upstream end of the i th axial mesh

x_d = downstream end of the i th axial mesh

The differential quotient of a function f(x) in the axial mesh is approximated by:

- 28 -

$$\frac{\partial}{\partial x} f(x) \approx \frac{\Delta f}{\Delta x} = \frac{f_d - f_u}{\Delta x} \tag{70}$$

f_d = value of the function f at the downstream end of the axial mesh

f_u = value of the function f at the upstream end of the axial mesh

The contribution of an axial mesh to an integral of the function f(x) can be approximated with the help of the trapezoidal rule:

$$\int_{a.m.} f(x)dx \approx 1/2 \cdot (f_u + f_d) \cdot \Delta x \tag{71}$$

8.3 Iterative procedure

In a closed loop we have the periodic boundary condition (18) for the bulk concentration of a solute i, but we have in general no a priori definite knowledge of the value at the origin of the loop x = 0. If there is a magnetic trap, which removes the solute quantitatively, we could take the axial position of the magnetic trap as the origin of the loop and we would then have the following condition:

$$c_i^b(x = 0) = C_{Fe}^{s,\,m.tr.} \tag{72}$$

The idea behind eq. (72) is that the iron concentration in the liquid metal in the magnetic trap can not fall below the thermodynamic equilibrium value. The magnetic trap acts primarily on iron particles and less on iron atoms. For the time being, the precipitation of iron or iron oxide particles in the liquid metal is not included in the code. But with eq. (72) we can describe the maximum effect that a magnetic trap can have.

The calculation of the bulk concentration and of the mass flux from the wall into the liquid metal along the whole loop would then be straightforward and the amount of solute removed in a time interval Δt by the magnetic trap would be determined by:

$$\Delta m_i^{rem.} = u^{fl} \cdot \Delta t \cdot A^{ch} \cdot (c_i^b(x = L) - c_i^b(x = 0)) \tag{73}$$

In all other cases one must proceed iteratively. The iterative procedure used in MATLIM is based on the following equation:

$$\int_0^L j_i(x) \cdot U_{ch} \cdot dx = 0 \tag{74}$$

which is an integral formulation of the mass conservation law; no solute disappears from the closed loop.

The following quantity can be calculated from the very beginning, as it depends only on the boundary conditions:

$$jc_i^w = \int_0^L K_i^{fl}(x) \cdot c_i^w(x) \cdot U_{ch}(x) \cdot dx \tag{75}$$

The iteration starts then with an initial value for c_i^b at $x = 0$. Then in a first round of iteration all the other values of c_i^b along the whole loop can be calculated with the help of eqs. (2) and (7). We can then calculate the following quantity:

$$jc_i^b = \int_0^L K_i^{fl}(x) \cdot c_i^b(x) \cdot U_{ch}(x) \cdot dx \tag{76}$$

Then we compare jc_i^w to jc_i^b by calculating the following quantity:

$$dev = ABS((jc_i^b - jc_i^w)/jc_i^w) \tag{77}$$

If the quantity dev is below a certain pre-defined threshold the iteration is finished, otherwise the value of $c_i^b(x=0)$ has to be changed and a new round of iteration starts. The number of iterative cycles N^{iter} is counted in the code. If no convergence is reached after a certain pre-defined number of iterative cycles N^{ult} the calculation is stopped and the whole iterative procedure must be changed somewhat.

8.4   Structure of the code

The global structure of the MATLIM code can be inferred from the following flow sheet:

Material data

Test data of the loop

Axial meshes

Temperature distribution along the loop, iron concentration at the wall

Selection of the mass flux model

Start of the iterative procedure for the mass transfer coefficient model

$N^{iter} = 1$

Iron flux, iron bulk concentration, oxygen bulk concentration

Convergence criteria fulfilled?

$N^{iter} = N^{iter} + 1$

$N^{iter} \geq$ iult ?

Transfer of the relevant results to output data set

Stop

The maximum number of iterative cycles is defined by the FORTRAN variable iult. This parameter can be specified by the user of the code. For the time being the default value of iult is 1000.

8.5 Steering variables

In the code MATLIM are included steering parameters, which enable the user to select the appropriate conditions. They are:

| icor | = | 0 | : | Pb-Li PICOLO loop |
| | = | 1 | : | LBE   CORRIDA loop |

| iox | = | 0 | : | no oxide scale present |
| | = | 1 | : | oxide scale present |

| itrap | = | 0 | : | no magnetic trap effect included |
| | = | 1 | : | magnetic trap effect included |

| itemp | = | 0 | : | low temperature case |
| | = | 1 | : | high temperature case |

9. Oxidation of martensitic and austenitic steels

In the test program for the behaviour of metallic components in a lead-bismuth environment austenitic, ferritic and martensitic steels have been investigated. In the test loop CORRIDA, which is of prime importance for us, specimens of martensitic steels are tested, but the tubing is of austenitic steel. Thus, our aim is to establish oxidation correlations for austenitic and martensitic steels for the range of temperatures and oxygen concentrations of interest to us. In order to reach this aim we need experimental data. As the data for steels in heavy liquid metal environment are rather scarce, we will check whether oxidation correlations gained for gas atmospheres can also be used for lead-bismuth. It has been stated by different authors (see for example [22] and [25]) that oxide scale formation under controlled gas atmospheres obeys the same principle mechanisms as in liquid lead or liquid

lead-bismuth alloy. Therefore it is interesting to compare oxidation rates obtained under gas atmospheres to oxidation rates in liquid metals.

In the following we will in case of gas atmospheres use the oxygen partial pressure p_{O2} and in case liquid metals the oxygen concentration. It should be noted that dissolution of oxygen in lead and also in lead-bismuth follows Sievert's law [33]:

$$c_o = K_{Pb-Bi} \cdot p_{O_2}^{1/2} \qquad (78)$$

K_{Pb-Bi} = Sievert's constant for lead-bismuth

The constant K can be calculated with the help of the following thermodynamic equation given in ref. [21]:

$$p_{O_2} = \frac{1}{a_{Pb}^2} \cdot \left(\frac{c_0}{c_{o,s}}\right)^2 \cdot \exp\left(\frac{2 \cdot \Delta G_{PbO}}{R \cdot T}\right) \qquad (79)$$

a_{Pb} = activity of Pb

$c_{o,s}$ = oxygen solubility in Pb-Bi

R = gas constant

ΔG_{PbO} = free energy for PbO formation

R = gas constant

9.1 Oxidation correlations for austenitic steels in gas atmospheres

No oxidation correlations for martensitic steels for the range of oxygen partial pressures relevant for LBE loops have been found for martensitic steels. There are data for oxide scale thickness under steam atmospheres to be found in ref. [34] but the oxygen partial pressure was not given. Also, this parameter was certainly far above the range in which we are interested. Thus, for the time-being we have only for austenitic steels oxidation correlations for temperatures at 550°C and higher.

The influence of the Cr-content on the oxidation behaviour in simulated steam has been investigated in ref. [35] for different commercial austenitic and ferritic/martensitic steel alloys and compared to the behaviour of Fe-Cr model alloys with systematic variations in their chemical composition from 9 to 16 wt% Cr for temperatures between 550 and 650°C. High chromium materials exhibited the best oxidation behaviour, whereas low chromium materials formed thick, multi-layered oxide scales, prone to spalling. Model alloys with high chromium content formed thin Cr_2O_3 layers in this temperature range. The weight gain of the model alloys remained

fairly high independent of the increasing Cr-content up to some critical value for this parameter, which increased slightly with increasing temperature from 11 to 14 wt%. No values for the oxygen partial pressure were given in ref. [35], but it seems that they were far above the range relevant for liquid lead-bismuth alloys. Nevertheless, these results can be considered as a sort of guideline for the interpretation of oxidation results in liquid metal environments.

The initial stages of oxidation of the ferritic steel P91 were studied at an oxygen partial pressure ranging from 10^{-11} to 10^{-8} bar in ref. [36]. It was found that there occurred surface segregation of minor alloying elements like silicon, phosphorous and nitrogen. Especially the formation of SiO_2 retards the oxidation of iron and chromium.

9.2   Correlations for duplex scale formation on austenitic steels

At 550°C and above double-layer oxide films, so-called duplex scales are formed on austenitic steels with Cr content below 18 wt% under gas atmospheres and also in a liquid LBE environment. It seems that the oxidation kinetics is independent of the oxidizing medium and does only depend on the oxygen partial pressure. At least we will in the following use this a working hypothesis. Therefore we will check whether we can use the correlations obtained from tests under gas atmospheres in static and dynamic lead-bismuth alloys.

In [37] vacuum annealed AISI 316 was oxidized under CO/CO_2 atmospheres at 600°C. It was found that the parabolic rate constant depended on the oxygen partial pressure in the following way:

$$k_p \propto p_{O_2}^{0.135} \tag{80}$$

In [38] AISI 316 was oxidized under a Ni/NiO oxygen buffer in the temperature range of 570 to 740°C. The observed oxygen partial pressure dependence was as follows:

$$k_p \propto p_{O_2}^{0.141} \tag{81}$$

In [37] the oxygen partial pressure ranged between about 10^{-25} and 10^{-15} bar and in [38] it ranged between about 10^{-22} and 10^{-18} bar. The exponents in (65) and (66) are fairly near together. As lead-bismuth loops are generally operated at oxygen concentrations of 10^{-2} wt % that means at an oxygen partial pressure of about 10^{-22} bar, the experimental data of Smith [37] and Saito [38] are very useful for us. In ref. [39] it is pointed out, that according to Wagner's oxidation theory a doubly charged vacancy transport mechanism would mean that the diffusion coefficient and also the

parabolic rate constant should vary with the oxygen partial pressure as $p_{O2}^{1/6}$. Thus, the oxide scale thickness should scale with $c_o^{1/6}$.

In [37] and [38] correlations for the weight gain Δw are given, but we are more interested in values of the oxide scale thickness, as this parameter is more easily accessible in post test examinations. Thus, our aim is to transform the parabolic rate constant for the weight gain k_p^m into the parabolic rate constant for the scale thickness k_p^δ.

$$\delta_{ox}^2 = k_p^\delta \cdot t \tag{82}$$

t = time in s

The weight gain for a duplex scale can be related to the thickness values of the subscales as follows:

$$\Delta w = \frac{4 \cdot M_O}{4 \cdot M_O + 3 \cdot M_{Fe}} \cdot \rho^{ma} \cdot (1 - P^{ma}) \cdot \delta^{ma} + \frac{4 \cdot M_O}{4 \cdot M_O + M_{Fe} + 2 \cdot M_{Cr}} \cdot \rho^{sp} \cdot (1 - P^{sp}) \cdot \delta^{sp} \tag{83}$$

M = atomic mass in g $\qquad$ δ = thickness in cm $\qquad$ ρ = theoretical density in g/cm^3

P = porosity

ma = magnetite $\qquad$ sp = Fe/Cr spinel

No information on internal oxidation was given in [37] and [38]. We have assumed that this contribution can be neglected.

It is an experimental fact that:

$$\delta^{ma} \approx \delta^{sp} \approx 1/2 \cdot \delta_{ox} \tag{84}$$

Also, we are certainly entitled to use:

$$\rho^{ma} = \rho^{sp} \tag{85}$$

and

$$P^{ma} = P^{sp} \qquad (86)$$

For the time being we have no experimental data on the porosity values in duplex scales. Therefore we set the porosity P equal to zero and we use for the theoretical density of magnetite the value of 5 g/cm^3. With these assumptions and values we obtain the following parabolic rate constants:

a)   Smith [37] at 600°C

$$k_p^\delta (p_{O_2}) = 0.7135 \cdot 10^{-10} \cdot p_{O_2}^{0.135} \qquad (87)$$

b)   Saito et al [38]

$$k_p^\delta (T, p_{O_2}) = 8.992 \cdot 10^{-4} \cdot p_{O_2}^{0.141} \cdot e^{-13708/T} \qquad (88)$$

P_{O2} in Pa   T in K k_p^δ in cm^2/s

In Fig. 4 are shown values of the oxidation rate constant according to (87) and (88) at a temperature of 873 K in the range of oxygen partial pressures between 10^{-24} and 10^{-21} bar. The values from both correlations are near together. A question arises about the lower limit of oxygen partial pressure for duplex scale formation. It seems that at very low oxygen partial pressures thin (about 1 µm), protective, and dissolution resistant oxide layers are formed [40]. As can be taken from the Richardson-Ellingham diagram shown in ref. [41], the lower limit of oxygen partial pressure for magnetite formation is at about 10^{-26} bar at a temperature of 823 K.

In Fig. 5 and 6 are plotted values of the oxide scale thickness versus time calculated with the help of correlation (9) obtained from the data of Saito et al [36]for temperatures of 823 and 873 K with the oxygen partial pressure as a parameter. After 10000 h we have oxide scale thickness values of about 30 to 50 µm (873 K) and about 20 to 30 µm (823 K). That means these values seem to be in a reasonable range.
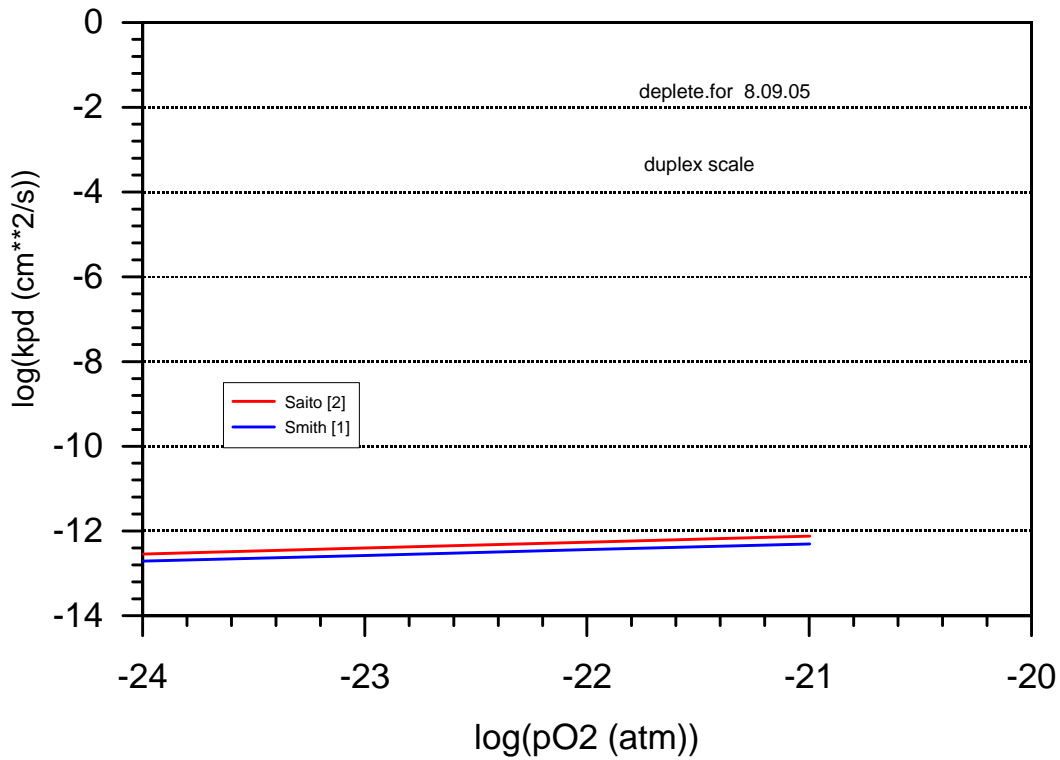
Fig. 4 Parabolic rate constant for growth of duplex scales versus oxygen partial pressure at 873 K
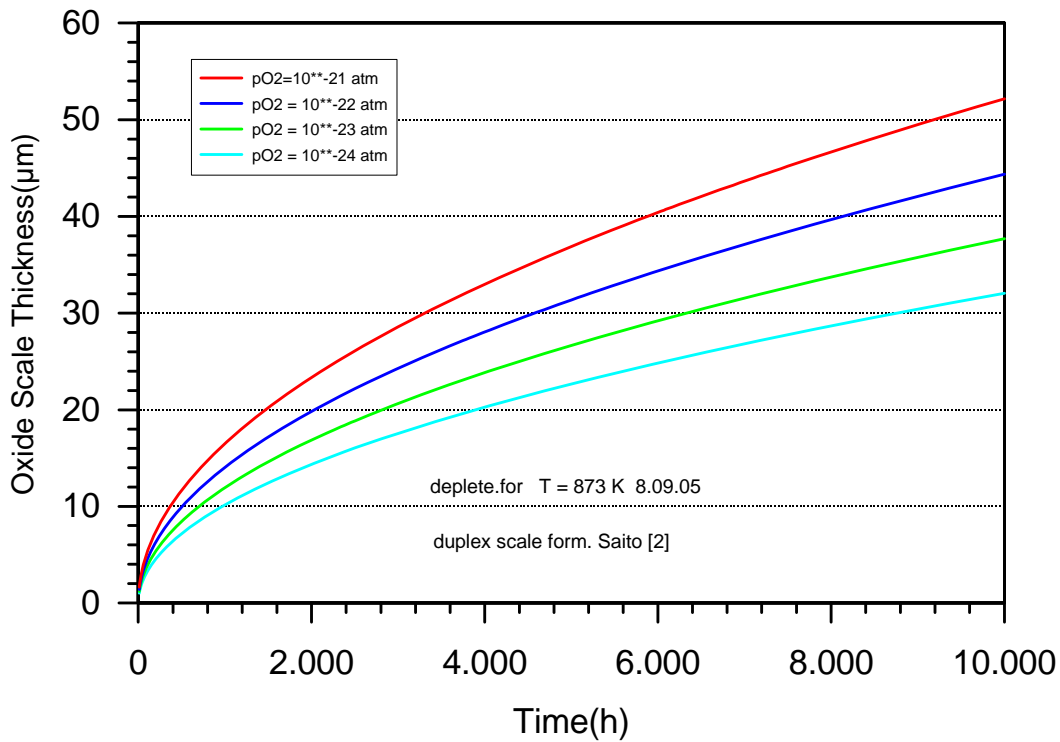

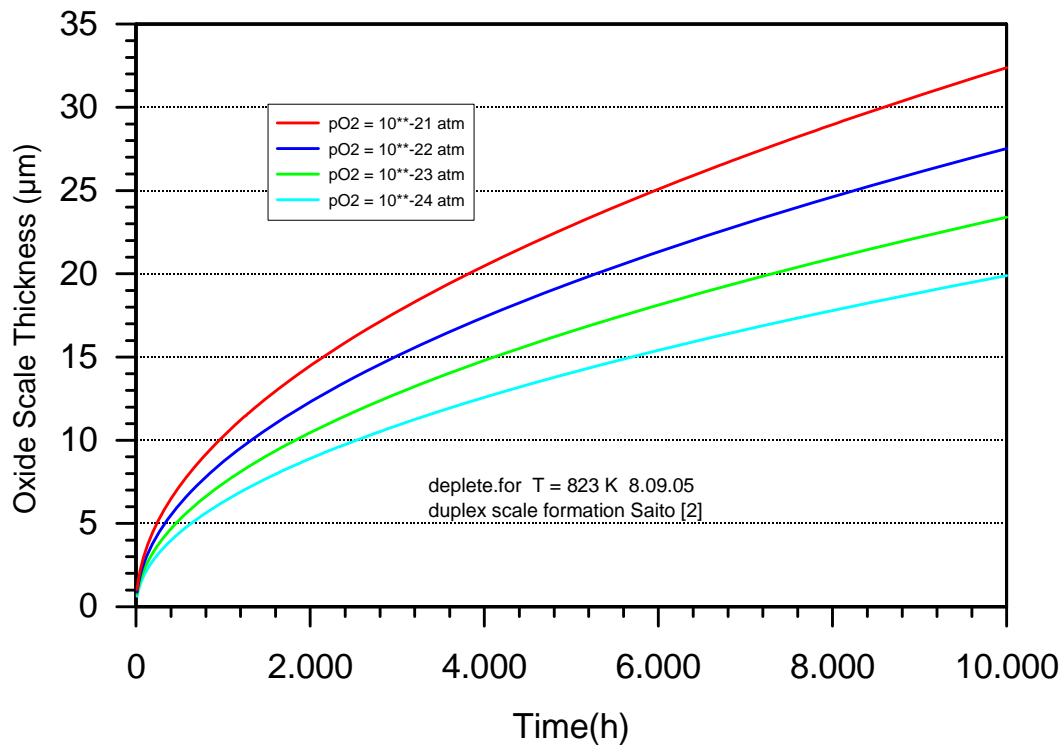Fig. 5 Evolution of the thickness of duplex scales for different values of oxygen partial pressure at 873 K

Fig. 6 Evolution of the thickness of duplex scales for different values of the oxygen partial pressure at 823 K

9.3 Oxidation results for martensitic and austenitic steels in liquid metals

We are mainly interested in the oxidation of martensitic and austenitic steels in lead-bismuth alloys. But as there are systematic studies of corrosion of steels in liquid lead are available in the literature, we will also have a short look on these results. Loops with Pb-17Li, on the other hand, are operated at very low oxygen contents in order to avoid the formation of Li_2O. Thus, the question of oxidation is irrelevant in this case. But the dissolution of oxide scales in Pb-17Li is certainly of importance.

9.4 Lead

It can be surmised that there is a wealth of data available in Russia on the corrosion of steels in liquid lead environments that has not been published in the open literature. In the recent years collaboration with western countries has been started resulting in valuable information on corrosion data (see for example [25, 43-46]). In the so-called Markov diagram (reproduced in ref. [25]) the corrosion depth of two

austenitic steels is plotted over a wide range of oxygen contents. Below a critical value of the oxygen content (about $10^{-7} - 10^{-6}$ at% oxygen) there is dissolution attack of the unprotected steel with dissolution rates of up to 200 µm in 3000 h. Above the critical range occurs oxide scale formation with the oxide scale thickness increasing logarithmically with the oxygen content. We have estimated that the parabolic rate constant scales with $c_o^{0.3}$ for the steel 15Cr-11Ni-3Si-MoNb and for the steel 16Cr-11Ni-3Mo with $c_o^{0.38}$. Thus, the exponent is distinctly higher than that for oxidation of austenitic steels under gas atmospheres (n=0.07). We think that this difference is to be attributed to the action of dissolution effects in liquid lead.

9.5   Lead-bismuth alloys

Experimental data for oxidation in lead-bismuth alloy are relatively scarce and the investigations having been done are not very systematic. No systematic variation of the temperature and the oxygen content in the liquid metal alloy, for example, has been done. There are investigations under static and dynamic conditions. In the latter case we have the problem of dissolution effect on oxide scales (see section 10). With a relatively high oxygen concentration this effect should be rather small but we think that at low oxygen concentrations, high test temperatures and high flow velocities the dissolution effect can become rather important and as we are interested in the unperturbed oxidation values this represents a problem. We should also note that there could have been spalling of oxide scales, an effect which was not always clearly identified and noted in the reports.

We have collected the values of oxide scale thickness found in the literature (see refs. [20, 22, 25 and 46-57]). A considerable spread of data for the same test time was observed in some cases (see for example ref. [22]). We think that in such cases the lower value is probably due to spalling of the oxide scale. Thus, we have taken only the upper value. It should also be noted that we have not included cases with surface treated steel specimens, as the scale thickness is then very small.

We have calculated experimental values of the oxidation rate constant K_p^{exp} in the following way:

$$K_p^{exp} = (\delta_{ox}^{exp})^2 / t^{exp} \tag{89}$$

t^{exp} = operation time

If several values of oxide scale thickness for different test times were available, we have calculated the time averaged value of the oxidation rate constant for the whole test series.

Data for ferritic/martensitic steels for temperatures of 470-480 and for 550°C are shown in Figs.7–10. It is evident that oxidation correlations would be specific for each type of steel. There is probably no global oxidation correlation for all martensitic steels, which would describe the behaviour in a precise way.

We had expected that tests under static conditions would provide values of oxide scale thickness at least as high as that from dynamic conditions (for the same steel

and at the same conditions of temperature and oxygen concentration). This is not always the case.

Based on the results for gas atmospheres we would have expected that at 550°C the oxidation rate constant for duplex scale forming steels should scale with $c_o^{1/3}$. As can be taken from Fig. the oxidation rate constant for Optifer, HT-9 and F82H scale with about $c_o^{0.5}$. That the oxidation rates under dynamic conditions for P122, ODS and Manet are fairly below is not surprising as at such low oxygen concentrations the dissolution rate may be no longer negligible (see also Section). The very low oxidation rates for P122 and ODS under static conditions (Müller et al refs. [51-53]) may be caused by periodic spalling of the oxide scale and eventually due to problems with the oxygen control.
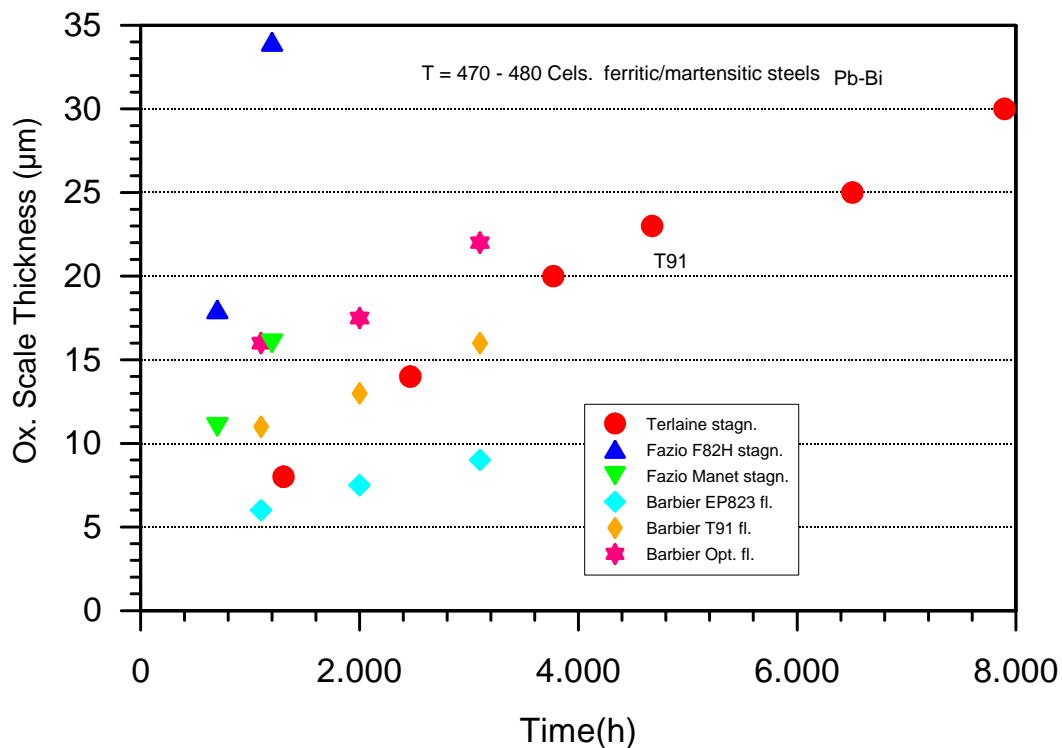

Fig.7 Experimental values of oxide scale thickness versus time for ferritic/martensitic steels tested in Pb-Bi at temperatures of 470 – 480°C
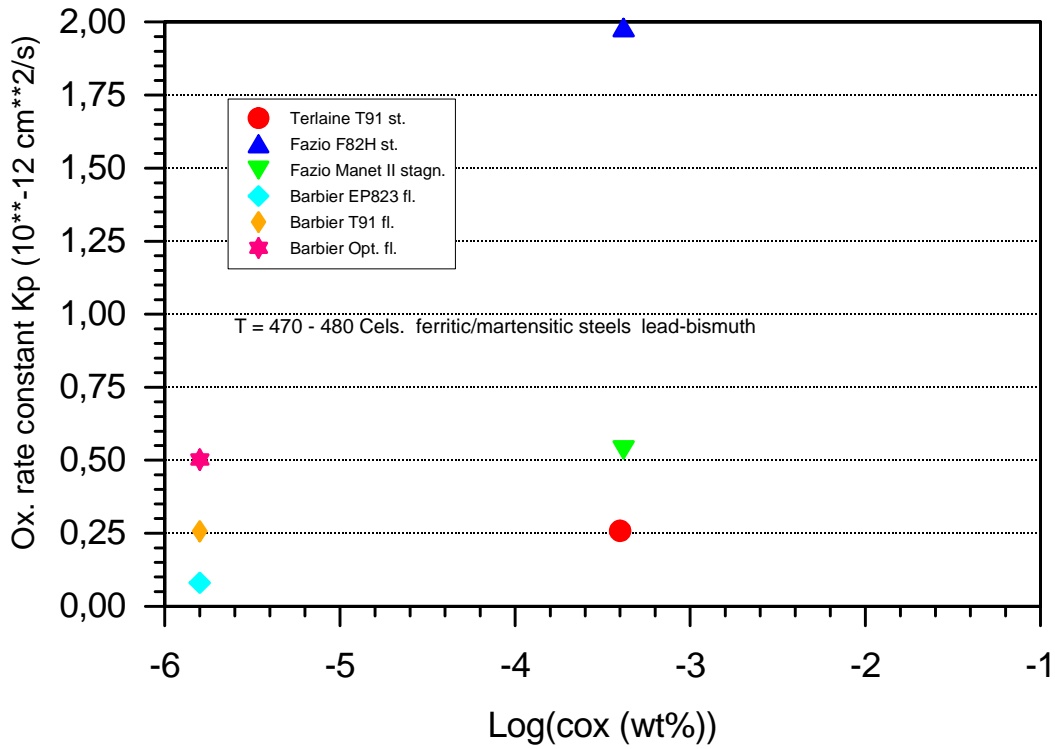
Fig.8 Experimental values of oxidation rate constant versus oxygen concentration for ferritic/martensitic steels tested in Pb-Bi at temperatures of 470 – 480°C
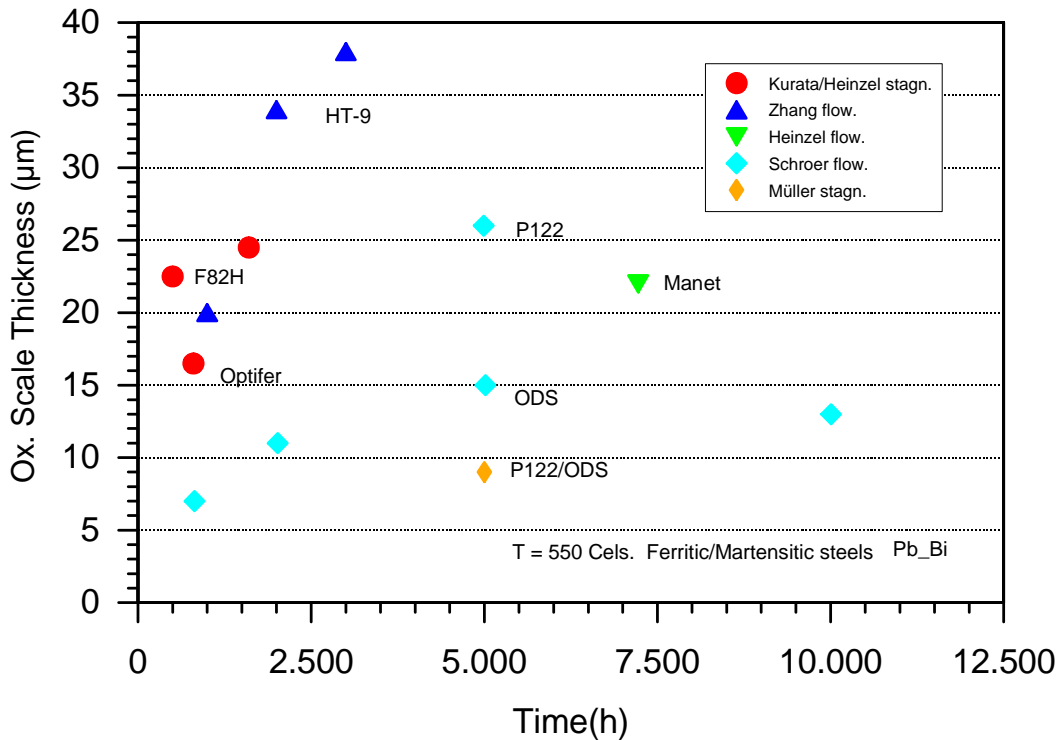

Fig.9 Experimental values of oxide scale thickness versus time for ferritic/martensitic steels tested in Pb-Bi at temperatures of 550°C
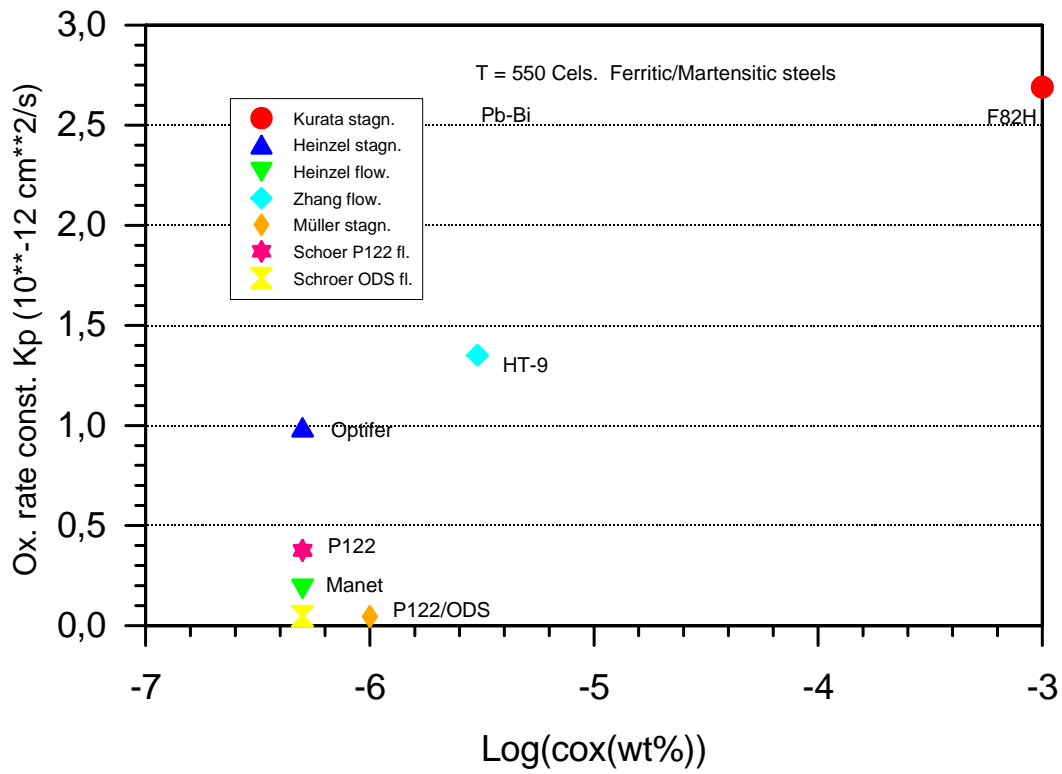
Fig.10 Experimental values of oxidation rate constant versus oxygen concentration for ferritic/martensitic steels tested in Pb-Bi at temperatures of 550°C
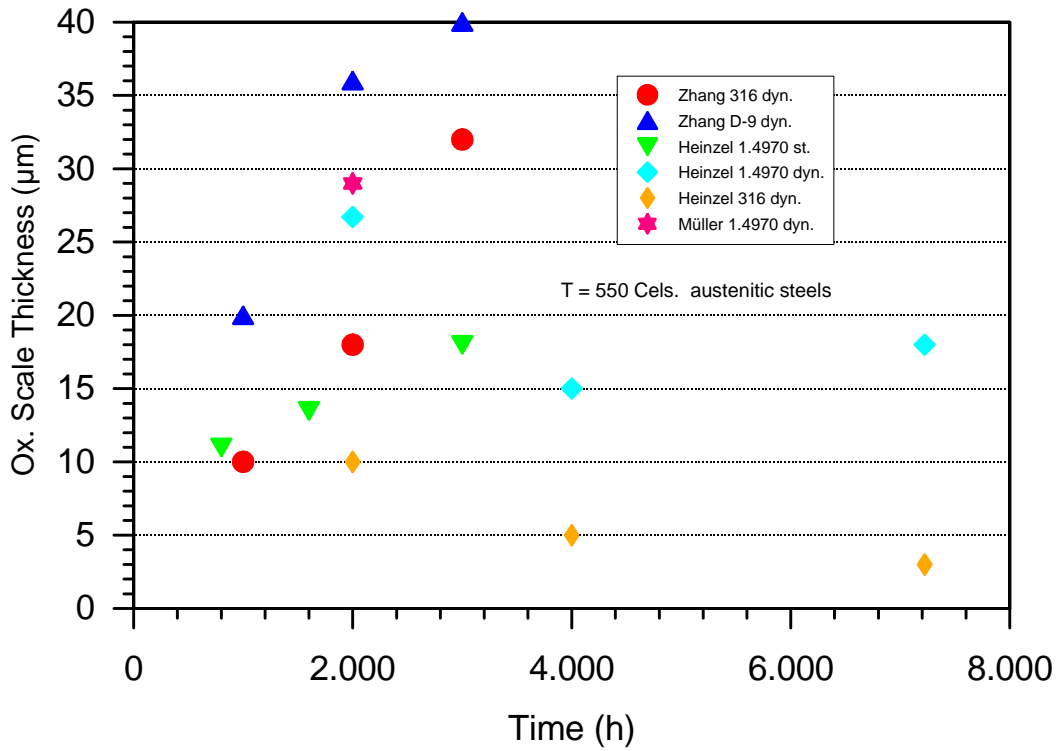
Fig.11 Experimental values of oxide scale thickness versus time for austenitic steels tested in Pb-Bi at temperatures of 550°C
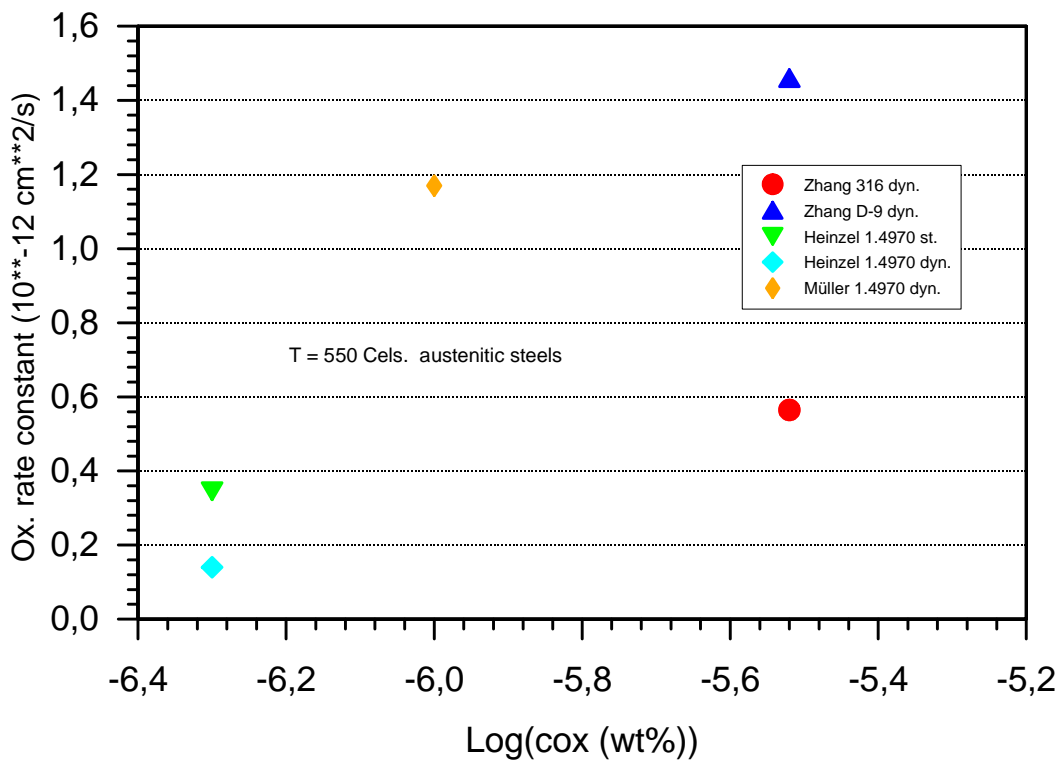

Fig.12 Experimental values of oxidation rate constant versus oxygen concentration for austenitic steels tested in Pb-Bi at temperatures of 550°C

It was found for austenitic steels that for temperatures up to about 470 – 480°C thin protective oxide scales are formed for saturated oxygen [54] as well as for low oxygen contents (0.001 – 0.0001 ppm) [53] under static and dynamic conditions [56].

Experimental data for oxidation of austenitics in Pb-Bi environments were mainly obtained for temperatures of 550°C and higher (see Figs. 11 and 12). There are some results gained at 420°C mentioned in ref. [56], but no values of the oxide scale thickness were given. In any case the oxide scales are rather thin and there seem to be no problem with dissolution attack. Therefore we have represented only the data at 550°C.

The rule that the oxidation rate constant increases with the oxygen content in the liquid metal seems to be well obeyed, although with the scarcity of data it is not possible to determine the exponent of c_o.

There are some results for austenitic steels under dynamic conditions in lead-bismuth at 600°C reported in ref. [20]. Part of the surface of the specimens was covered by thin and thick oxide scales and there were locations of dissolution attack by the liquid metal. This behaviour of austenitic steels at high temperature was explained in ref. [20] by the decrease of the oxygen activity with increasing temperature. We, on the other hand, think that it is due to debonding and later on spalling of the oxide scales. A viable scenario for local dissolution attack might be as described in the following. If there occurs debonding of the oxide scale, infiltration of liquid lead-bismuth into the gap between the metallic substrate and the oxide scale by capillary effect seems likely. The amount of oxygen within the liquid metal may be insufficient for oxide scale formation but diffuse into the metallic substrate enabling the onset of dissolution attack. This might then prevent from anew oxide scale formation after spalling of the oxide scale.

Results of oxidation of AISI 316 under gas atmospheres between 843 and 1010 K are reported in ref. [38]. It was found that the oxidation rate increases with temperature over the whole temperature range. Remains of thick oxide scales found in [20] demonstrate that this should also the case in lead-bismuth alloys. The observation of locations with thin oxide scales and locations of dissolution attack should be a consequence of oxide scale debonding and spalling.

In order to calculate the lower bound of the oxygen partial pressure for magnetite formation the following thermodynamic relationship is used [23]:

$$p_{O_2}^{l.b.ma.} = \frac{1}{a_{Fe}^{3/2}} \cdot \exp(\frac{\Delta G_{Fe_3O_4}}{2 \cdot R \cdot T}) \tag{90}$$

But it should be noted that in a non-isothermal loop we are not in a situation of thermodynamic equilibrium and that the magnetite scale is not directly formed on the steel but that there is Fe/Cr spinel layer in between. In ref. [20] it is reported that martensitic steels form duplex scales even at low temperatures of 420°C, whereas in ref. [49] only simplex spinel layer formation has been observed, although in both cases the same nominal value for the oxygen concentration was reported. The oxygen concentration in ref. [49] was in the first half of the operation at very low

values during extended periods and during the second half it oscillated around the nominal value.

In ref. [22] values of the magnetite subscale thickness have been calculated with the help of the mono-crystalline Fe tracer diffusion coefficient of Dieckmann and Schmalried [42]. Using the following equation:

$$\delta_{ox} = 1.91 * \delta^{ma} \qquad (91)$$

values for the duplex scale thickness could be obtained. But there are short circuit paths like grain boundaries and pores for the diffusion of iron in the magnetite, whose contributions cannot be estimated, we think that a procedure for the calculation of duplex scale thickness values based on experimental data is better suited for our purposes. It is also simpler than the procedure in ref. [22]. Also, the agreement between experimentally determined values and calculated ones was not so good in ref. [22].

As a rule of thumb it can be stated that the values of oxide scale thickness and the oxidation rates observed in liquid lead-bismuth alloys are in the same range as that obtained under gas atmospheres.

10. Experimental indications for dissolution effects on oxide scales in stagnant and flowing lead-bismuth alloys

The possible dissolution of oxide scales in heavy liquid metals is a generic issue. In Pb-17Li loops like PICOLO, which are operated at very low oxygen contents, there is no doubt about such an effect. It is presumably responsible amongst other causes for the so-called incubation effect. This is due to the fact that pre-existing oxide scales are much more difficult to dissolve than bare metallic surfaces. In lead-bismuth alloys on the other hand the question of oxide scale dissolution is unresolved. We think that we have found in the literature indications that for low oxygen contents there may be a sensible effect, which could be of technological importance.

As is well-known, under gas atmospheres every substance has a vapour pressure. In a liquid environment the vapour pressure is to be replaced by the solubility. Thus, we believe that every substance has in liquid metals non-zero solubility. For most oxides the solubility will be very small, but for magnetite it could be non-negligible. A good example is also provided by PbO itself. At the saturation point Pb_{sol} coexists with solid PbO. With oxygen contents below saturation all PbO will be dissolved.

There is no doubt that oxide scales are dissolved by liquid LBE at low oxygen concentrations. Results of corrosion tests on as-received and pre-oxidized specimens of the martensitic steel F82Hmod in stagnant lead-bismuth under isothermal conditions at 400 and 600°C are, for example, reported in ref. [57]. The oxygen concentration in the lead-bismuth for the non-inert device was estimated to be approximately 10^{-8} wt%. The pre-oxidized specimens showed weight losses as well as the as-received specimens. These weight losses increased with temperature. In ref. [20] it is reported that at an oxygen concentration of 6 10^{-8} wt% in stagnant

LBE at 550 $^{\circ}$C there was no oxide scale formation but dissolution attack, whereas for an oxygen concentration of 5 10^{-7} wt% oxide scale formation was observed. But it should be noted that at temperatures of 550 ^{0} C and higher there could occur in flowing LBE heavy dissolution attack of the steel components for relatively high oxygen concentrations of 0.03-0.05 ppm (see for example ref. [22] and [55]), which are normally sufficient for oxide scale formation on stainless steels. One explanation might be that in a first stage there occurred oxide scale formation and then at a critical oxide scale thickness debonding and spalling of the oxide scale. Why there didn't occur renewed oxidation at these locations but dissolution attack is an open question.

We think that in lead-bismuth alloys diagrams similar to the Markov diagram in lead (see for example ref. [25]) could be established, where two regimes could be distinguished, namely a dissolution regime and a regime of oxide scale formation depending on the oxygen content in the liquid metal. A pre-oxidized specimen exposed to the liquid metal in the dissolution regime would suffer complete dissolution of the oxide scale and thereafter dissolution attack of the metallic substrate. We also think that in the oxidation regime we have simultaneously oxide formation and dissolution with oxide formation being the dominant mechanism.

The value of the critical oxygen partial pressure for magnetite formation is given by [22, 23]:

$$p_{O_2}^{1/2}(T) = \frac{1}{a_{Fe}^{3/4}} \cdot \exp(1/4 \cdot \Delta G_{Fe_3O_4}^s /(R \cdot T)) \tag{92}$$

ΔG_{Fe3O4} = Gibb's free energy of formation for magnetite

For oxygen partial pressures below this critical value magnetite scales will certainly be dissolved. But there may be also a dissolution effect above this critical pressure value.

The dissolution rates of oxide scales have never been determined experimentally. We follow the position adopted in ref. [23] that the oxide film is subjected to reduction by the liquid metal if the concentration of Fe in the liquid metal is too low. It is very important now to consider the situation in a non-isothermal system, as there can be precipitation in the cold leg there is then dissolution in the hot leg of the system. Thus, the temperature difference constitutes the driving force for mass transfer. It was concluded in ref. [22] that the effect for oxygen concentrations of 0.01 ppm and higher is small. But if the value of the oxide scale dissolution rate is about 5 µm/y for values of the oxygen content of 0.03 − 0.05 ppm (as reported in ref. [22]), we would expect it to be in the range of about 50 µm/y for an oxygen content of about 0.005 ppm.

It was found in ref. [47] that the oxide scale consisted of a single Fe/Cr spinel layer. For test durations of 10000 h we would expect in case of magnetite a value of about 30 µm for the recession rate of the metallic substrate due to dissolution effects. It should then be possible to determine this value experimentally. In case of Fe/Cr spinel our expectation is that dissolution rates should be distinctly lower. But then we have a problem with the evolution of the oxide scale thickness observed in ref. [49],

namely that it is not at all reminiscent of a parabolic behaviour but looks like a solution of Tedmon's equation. In ref. [50] it is reported for a duplex scale found after a test operation of 1200 h that the flowing LBE had eroded the scale by about 3 - 5µm, which would correspond to a rate of about 20 - 30 µm/y.

Weight losses are reported in ref. [54] for martensitic and austenitic steel specimens tested in flowing lead-bismuth at 470 and 600°C. These weight losses were attributed in ref. [55] to erosion, but no experimental evidence was given to support this interpretation. We think that in case of stable oxide scale formation the weight losses were presumably due to oxide scale dissolution. At the lower temperature important weight losses occurred only for the tests done at rather low oxygen content (10^{-7} -10^{-8} wt%), a condition favourable for the dissolution effect. With the data given in [52] we have estimated the dissolution rates to range between 5 and 50 µm/y in the low temperature case. At 600°C the estimated dissolution rates can become as high as 80 µm/y. Weight losses can, of course, also result from oxide scale spalling. But we have got the impression that the oxide scales in ref. [55] were mechanically stable.

In case of duplex scale formation we think that as rule the thicknesses of both subscales are roughly equal (see for example ref. [22]).This would mean that the location of the oxide/oxide interface is roughly identical with the original surface of the metal. If the thickness of the magnetite subscale is distinctly smaller than that of the Fe/Cr subscale, as for some cases observed in ref. [20], we consider this as indicative of dissolution effects on the magnetite.

11. Results of calculations for the PICOLO and the CORRIDA loop with the MATLIM code

In the turbulent flow regime the dissolution rates increase with a power of about 0.9 of the flow velocity, whereas in the laminar regime they would be independent of the flow velocity.

The CORRIDA loop is a multi-modular loop, it contains different components like two electrical reheaters, a heat exchanger, an air cooler, an oxygen control system, and two test sections with test specimens, all these modules have different hydraulic diameters and different geometrical dimensions. They are connected by tube sections. The treatment of multi-modular loops in the MATLIM code was described in section 7.1. A schematic view of the CORRIDA loop is to be found in fig.14.

A description of the CORRIDA loop can be found in ref. [58] and shall therefore not repeated in this report. Some characteristic numbers of the loop and basic material data assumed for the calculations are listed in Table. These calculations are to be understood as sensitivity studies under realistic assumptions for the situation in the CORRIDA loop.

Flow velocity at the test section	200 cm/s
Hydr. Diameter at the test section	1.2 cm
Temperature at the test section	550°C

Oxygen concentration	0.01 ppm
Iron diffusion coefficient	$1. \ 10^{-6} \ cm^2/s$
Length of the loop	3568 cm

Table Characteristic data for the calculations for the CORRIDA loop

There are no experimental data for dissolution and precipitation rates in lead-bismuth loops, especially in case of oxide scales present on the metallic components. But there are experimental values for dissolution rates available for lead-lithium loops like PICOLO. It was found by tests done in this loop, that at 480°C the dissolution rate was about 90 µm/y [59], and at 550°C it was about 700 µm/y both for a flow velocity of 30 cm/s. By calculations with MATLIM these experimental values could be reasonably reproduced for iron diffusion coefficients and using iron solubility data given by Feuerstein et al [26]. (see for example Fig.13 for the low temperature case). If one takes the solubility correlation of Coen et al [26, 27] for iron in Pb-17Li one has to assume values for the iron diffusivity in the range of $10^{-9} \ cm^2/s$ (see refs. [2] and [7]). Such values for the iron diffusivity are unreasonably low.

The dissolution rates in a loop are mainly determined by the product of the solubility and the mass transfer coefficient and one can estimate the dependence of the dissolution rates on the flow velocity in the loop and the diffusivity using the mass transfer correlation. The temperature dependence of the iron solubility is mainly although no exclusively responsible for the temperature dependence of the dissolution rates.
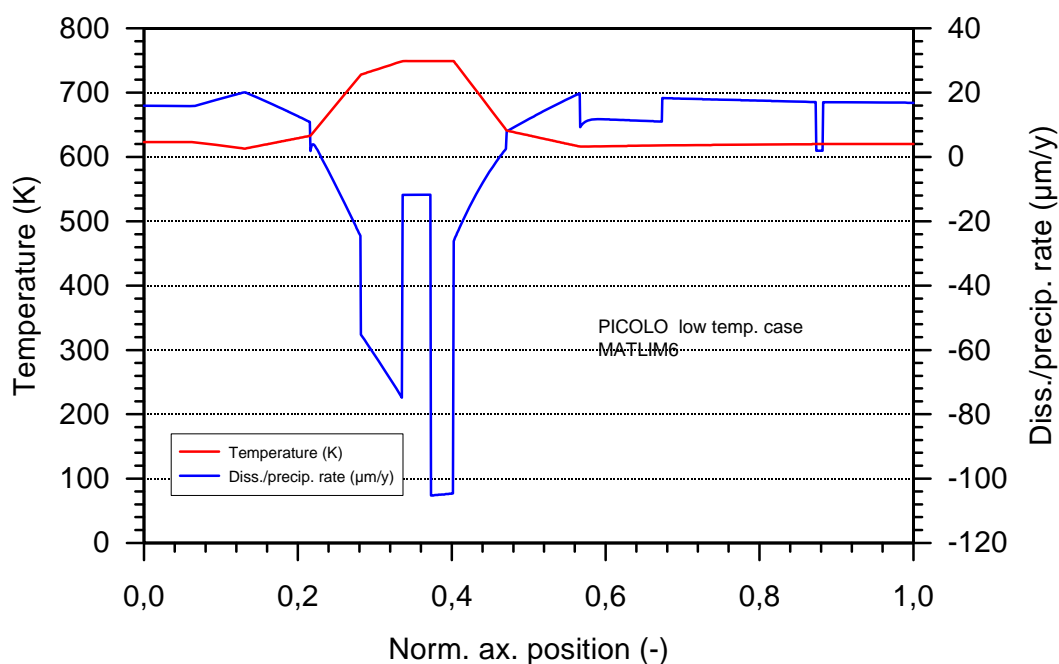

Fig.13 Calculated dissolution/precipitation rates in the PICOLO loop for a maximum temperature of 480°C

We think that the iron diffusivity in lead-bismuth alloy should be in the same order of magnitude as the iron diffusivity in lead-lithium. For this reason we have taken for the calculations for the CORRIDA loop a value of 1.10^{-6} cm^2/s for the iron diffusivity coefficient.

The dissolution rates of oxide scales are mainly determined by the solubility of metal atoms and the diffusivity. Hence, the choice of the relevant correlations is essential. In the following we consider only the dissolution effect on magnetite scales. The correlations given in ref. [3] seem most promising and have therefore been selected for this work.

Fig. 15 shows the axial profiles of the hydraulic diameter and of the flow velocity along the whole loop. The flow velocity has its highest value along the test sections loaded with the test specimens (200 cm/s).

Some of the results of the code calculations, which seem to be of greatest interest to the reader, are to be seen in Figs. 16–20 (maximum temperature in the loop about 550 K) . Most interesting are of course the dissolution/precipitation rates along the loop shown in Fig.18. It should be noted that due to the convention used in the MATLIM code negative values stand for dissolution and positive values for precipitation. The axial profiles of the dissolution/precipitation rates are rather perturbed for a multi-modular loop, a consequence of the hydraulic properties of the different components. The results plotted in Figs. 15-17 should help to understand these profiles, as the dissolution/precipitation rates are determined by the mass transfer coefficient and the difference between the iron concentration at the wall and in the bulk of the fluid. The mass transfer coefficient is mainly determined by the Reynolds and the Schmidt numbers. The maximum value of the dissolution rate (35 µm/y) is reached at the locations of the two test sections (short rectangles in fig.20). It should be noted that no experimental values for the dissolution rates of oxide scales are available and our calculations are to be understood as sensitivity studies. But we think that a value for the dissolution rate of 35 µm/y is in a reasonable range for the selected oxygen content of 0.01 ppm. The consequence of a variation of the Fe diffusivity is rather evident from the correlations of the mass transfer coefficient. For turbulent flow the dissolution rate would scale with $D_{Fe}^{0.6-0.7}$. This has been studied in ref. [1] and [2].

The flow is fully turbulent in the test sections and in the tubing sections of the loop but in some components like the air cooler, and electrical heater the Reynolds number is below 10^4 and the flow is therefore in a transition regime. Due to the low values of the iron diffusivity the values of the Schmidt number are rather high, they range between about 1200 and 1600. The mass transfer coefficient varies between 10^{-3} and 10^{-2} cm/s.

Figs. 18and 19 show the iron concentration at the wall (CFEW), the iron concentration in the bulk (CFEB) and the iron flux from the channel wall into the liquid metal. Negative values of the iron flux mean that the flux is directed from the liquid metal to the wall, leading to precipitation at the wall.

We believe that oxide scale formation in flowing lead-bismuth is determined by concomitant oxidation growth and dissolution. If the unperturbed growth of the scale can be described by a parabolic law, than the combined effect can be described with the help of the following differential equation (Tedmon's equation [10]):

$$\frac{d}{dt}\delta_{ox} = \frac{a_{ox}}{\delta_{ox}} - b_{ox} \tag{93}$$

a_{ox} = parabolic oxidation rate constant $a_{ox} = \frac{1}{2} * K_p$

b_{ox} = dissolution rate

In order to explore this differential equation we have done sensitivity studies. The results of such a study are to be seen in Fig.21. It is evident that the higher the dissolution rate the smaller will be the oxide scale thickness reached after a certain time. It has been discussed in section that with the presence of dissolution rates the oxide scale thickness will tend towards an equilibrium value. Effects of dissolution rates can probably only be detected for values above 10 µm/y and this only for longer operational times. A pre-requisite for eq. (93) is that the oxidation without dissolution is parabolic. But this condition is not always fulfilled (see for example refs. [21, 40]. At low oxygen content in the liquid metal a thin dissolution resistant Fe/Cr spinel oxide scale forms. Later on with higher oxygen content in the liquid metal one obtains local oxidation. It is not yet clear how such a situation can be treated analytically.

One effect of dissolution rates is not evident from Fig.19, namely the oxide scale moves inwards with a velocity at just half of the dissolution rate. That means we would get a recession of the metallic substrate higher than suggested by the thickness of the oxide scale itself. Thus, the dissolution rate could at best be determined via the recession of the metallic substrate. We are fully aware that we have described here an ideal situation. In reality we have scatter of the experimental data and it is by no way sure that the unperturbed oxidation is really parabolic or we have poor knowledge of the parabolic rate constant. We can also have spalling (partial or total) of the oxide scale and renewed oxidation. The new oxidation rate might even be higher than the old one due to Cr depletion effects. Thus, it might be difficult to identify a spalling event. Eq. (93) can, in principle, also be applied in this case, one only has to start in the time increment after the spalling event with the appropriate value of the oxide scale thickness. The propensity of the oxide scale for delamination and spalling increases with the thickness of the scale. Thus, a high dissolution rate b_{ox} should be beneficial with respect to mechanical effects.

In ref. [22] it is reported that on rod specimens made of AISI 316L only single-layer oxide films have been observed at 550°C and that this single layers could not prevent the specimens from local heavy liquid metal dissolution damage. As small pieces of oxide scale have been found, one can surmise that spalling has occurred either due to thermal cycling or at constant temperature due to growth stresses. But it is difficult to understand, why after a spalling event no new oxide scale is formed even if the oxygen content in the liquid metal is relatively high as given in ref. [22]. It seems that under certain circumstances Tedmon's equation for oxide scale formation [10] cannot be applied. In ref. [40] on the other hand stable protective albeit thin oxide scales have been found for rather low oxygen concentrations. We do not know the dissolution rates in this case, but we think that they are non-negligible and we think that Tedmon's equation can be applied in this case.
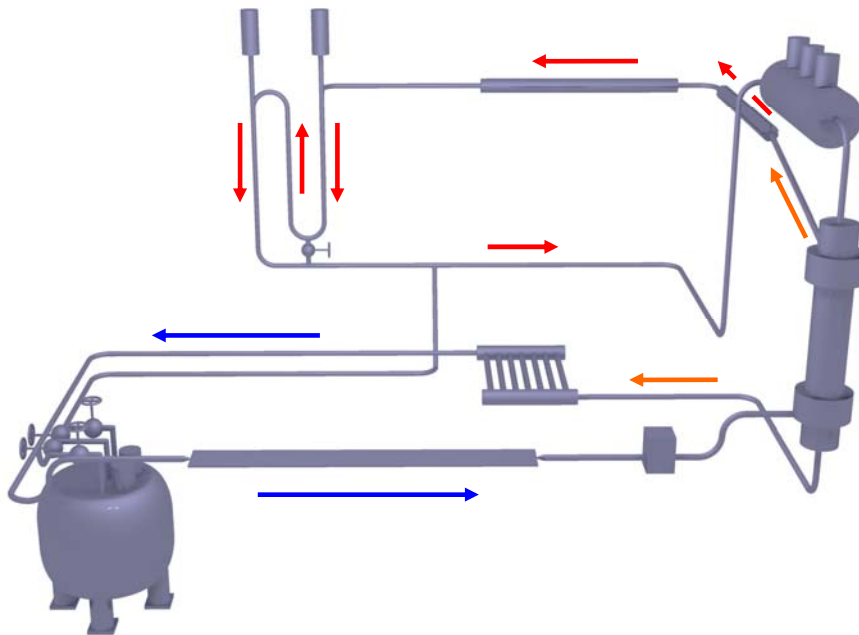
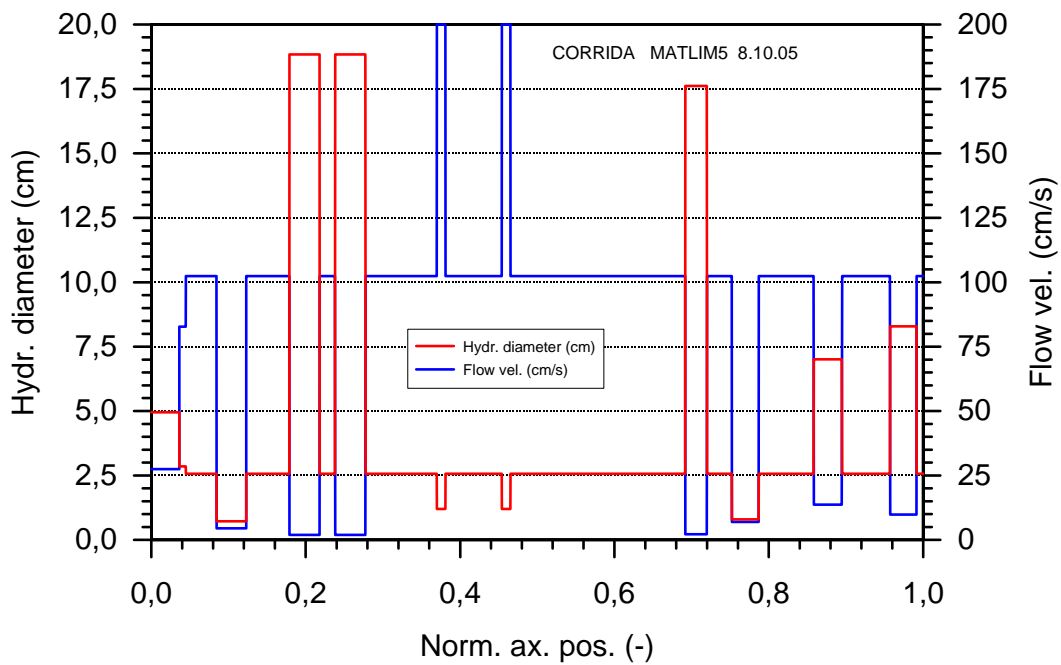Fig.14 Schematic view of the CORRIDA loop

Fig. 15 Axial profiles of the hydraulic diameter and the flow velocity for the CORRIDA loop
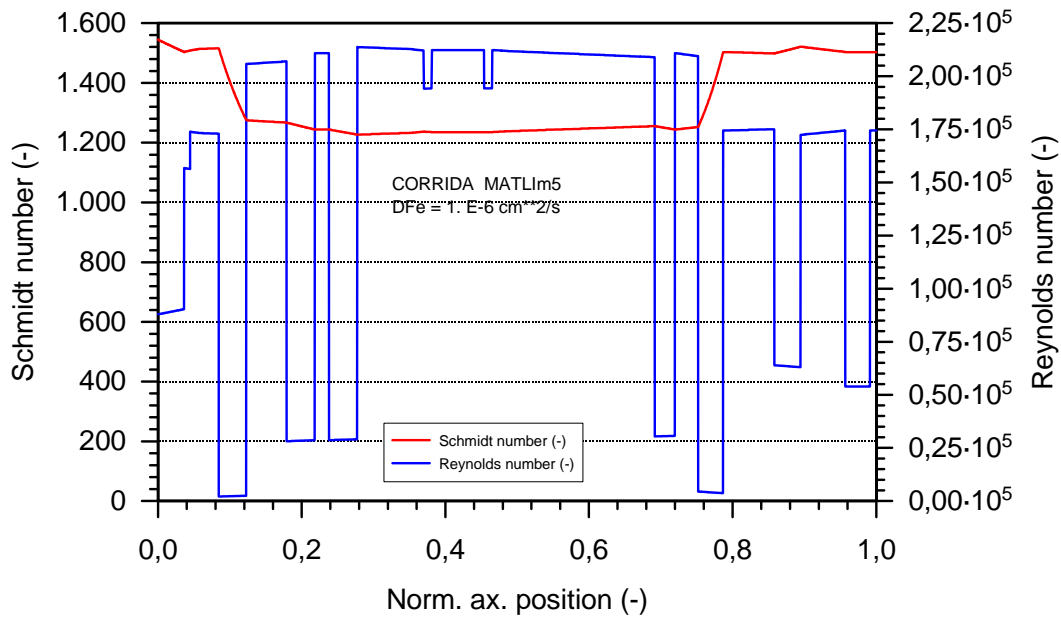
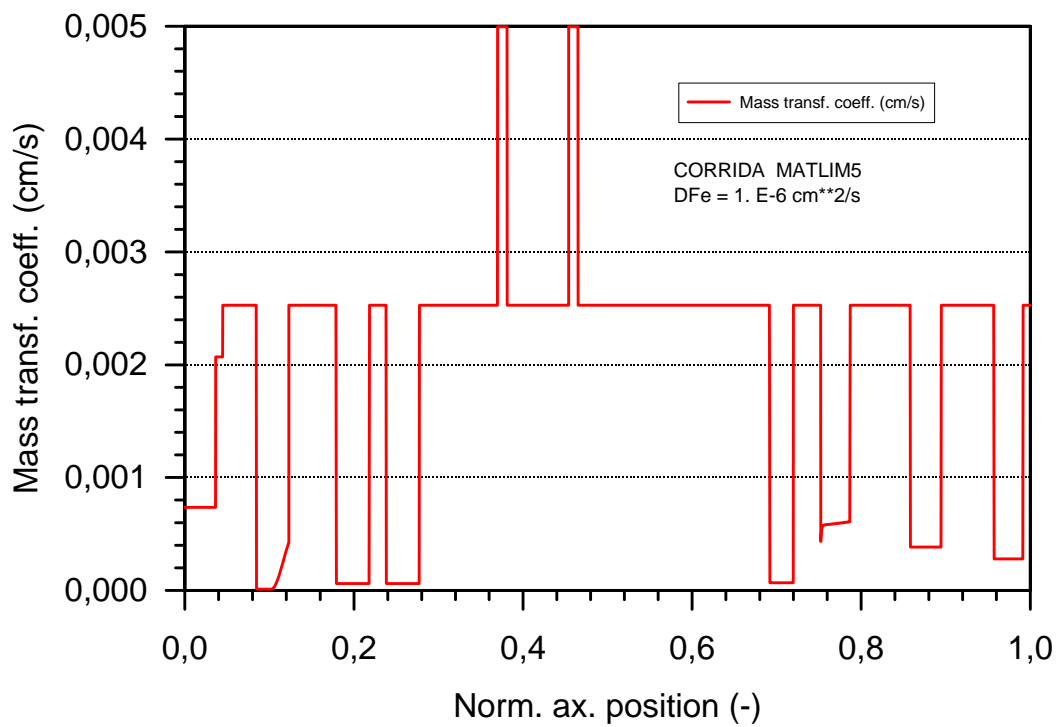Fig.16 Axial distributions of the Reynolds and of the Schmidt number

Fig. 17 Axial distribution of the iron mass transfer coefficient
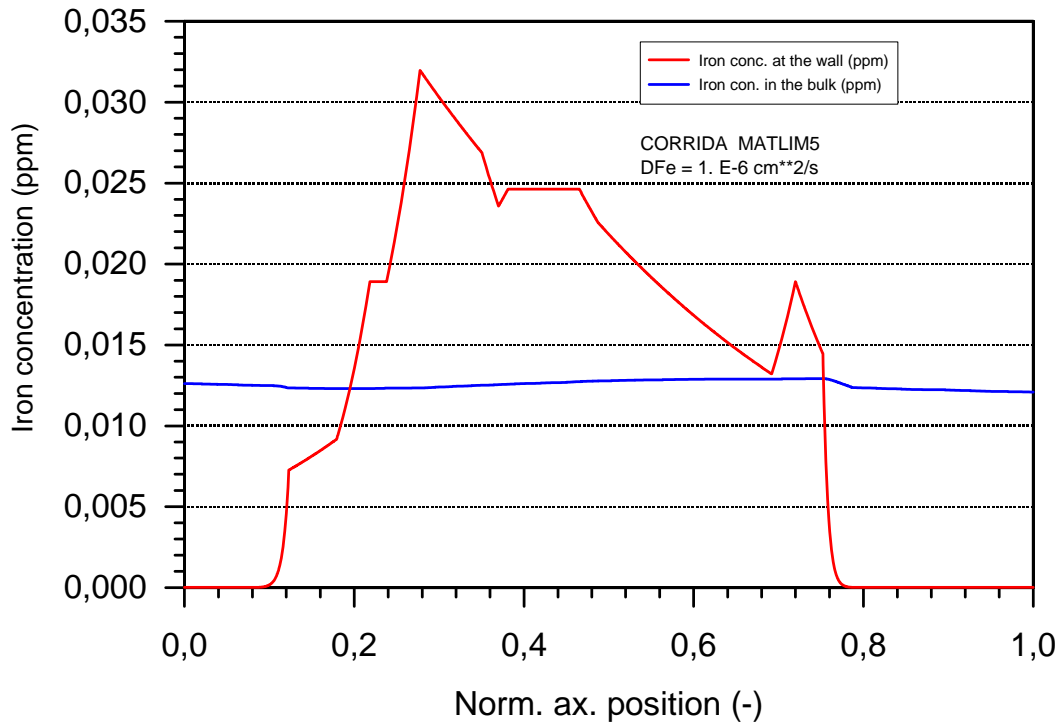
Fig18 Axial distributions of the iron concentration at the channel wall and in the bulk of the fluid
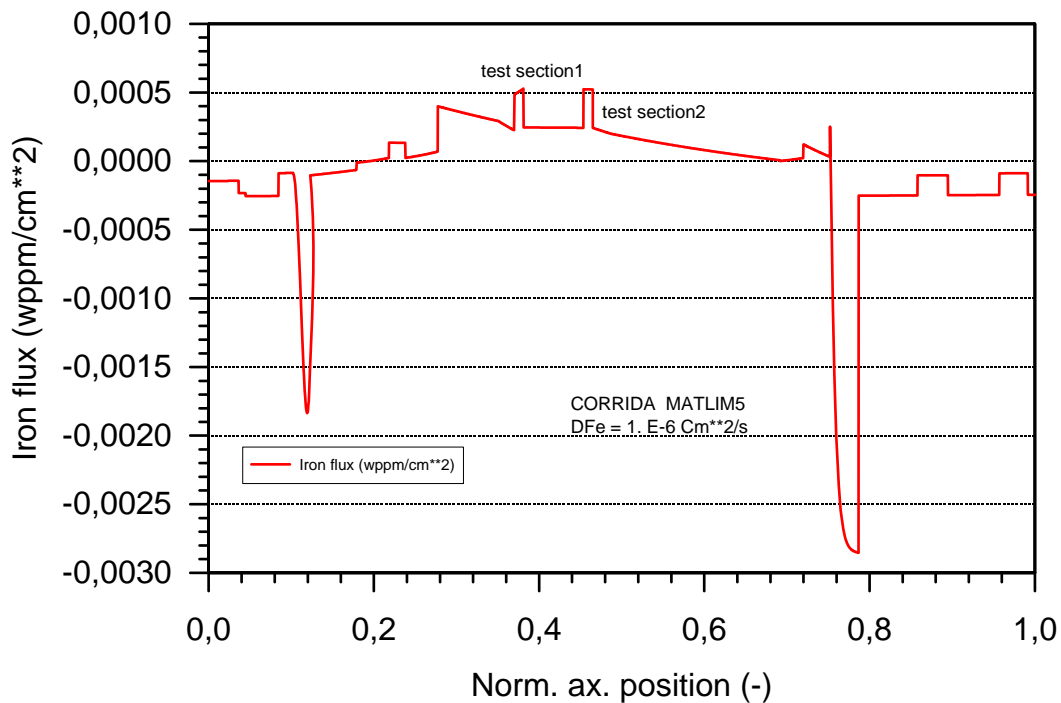

Fig19 Axial distributions of the iron flux from the channel wall into the liquid metal
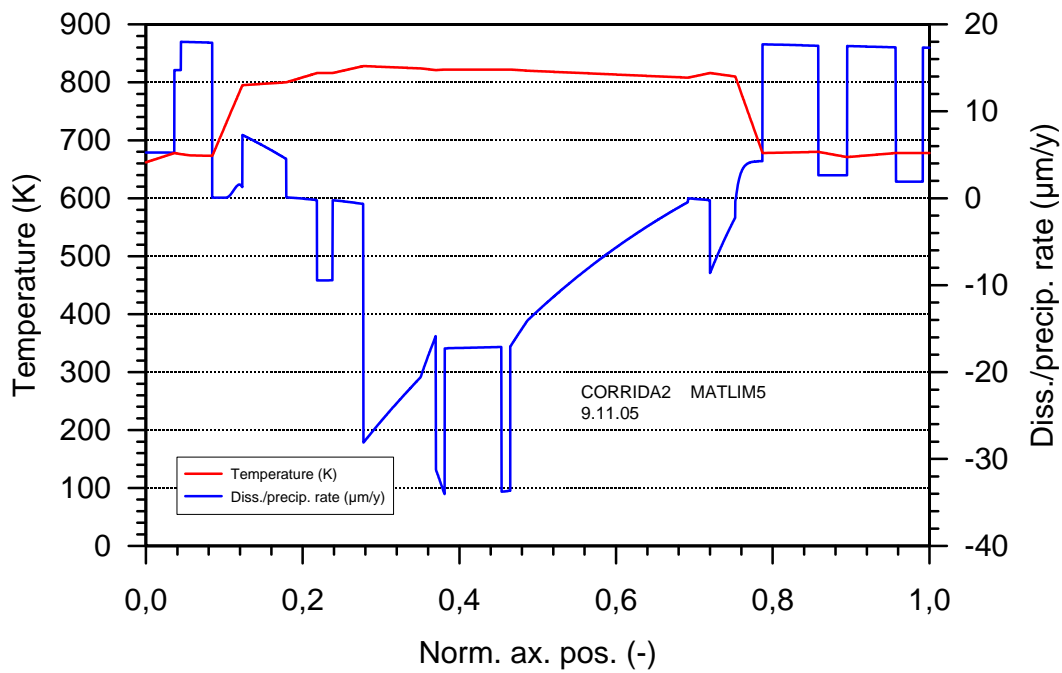
Fig.20 Axial distributions of the temperature in the CORRIDA loop and of the dissolution/precipitation rates
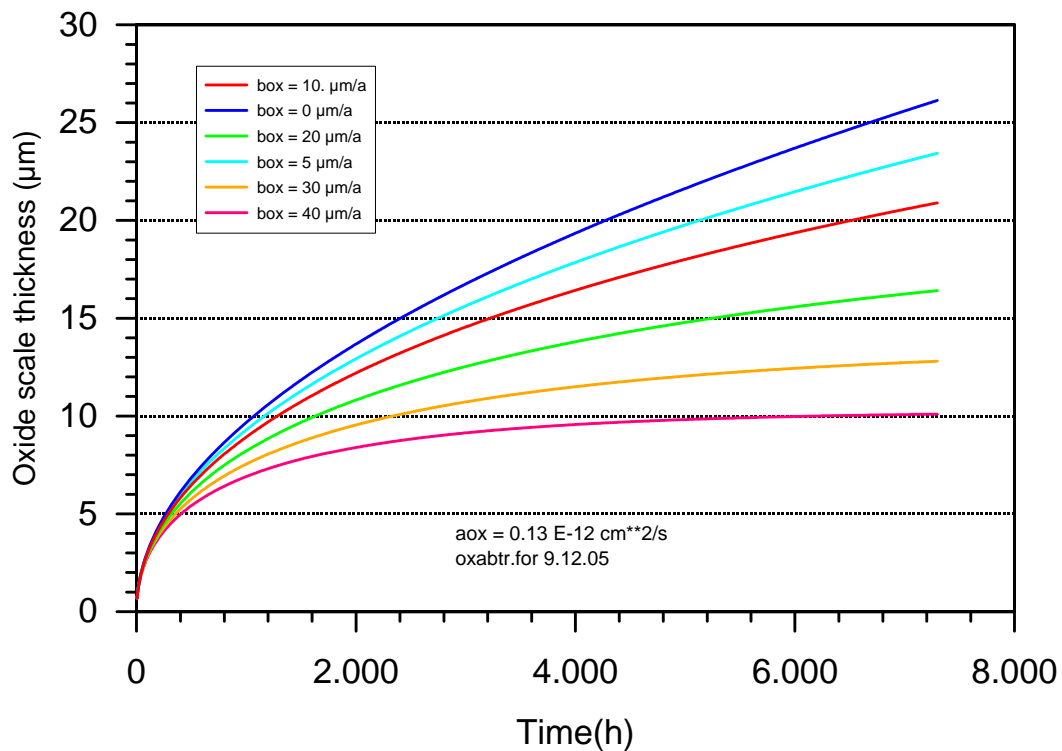

Fig.21 Evolutions of oxide scale thickness for different values of the dissolution rate b_{ox} (0 – 40μm/y) for a parabolic rate constant a_{ox} of 0.13 10^{-12} cm^2/s

12. Conclusion

A kinetic model for the calculation of mass transfer in liquid metal systems under forced convection flow conditions has been developed. It is based on the use of the relevant characteristic thermo-hydraulic numbers, which determine the mass flux from the wall into the fluid. This is supplemented by the application of the mass conservation law to calculate the conditions in the bulk of the fluid. The dissolution/precipitation rates determine then the geometrical changes of the structural components. For metallic surfaces the dissolution rates can be considerable. In this case a lot of experimental data are available. If oxide scales are present the dissolution rates should be very much smaller. Besides the thermo-hydraulic parameters like flow velocity and hydraulic diameter, iron diffusivity and solubility are of the greatest importance.

In a new round of calculations for the CORRIDA loop we have done sensitivity studies to test the new multi-modular version of the code MATLIM. For this we have used correlations for the iron solubility found in the literature. These correlations yield reasonable results for the dissolution rates. With the code MATLIM a simple and flexible tool for the calculation of mass transfer and geometrical changes in liquid metal loops is now available at FZK.

Concerning oxidation of martensitic and austenitic steels in lead-bismuth alloys under static and dynamic conditions we have looked through the literature and collected the relevant data. We are not yet in a position to establish oxidation correlations as the data are rather scarce in view of the many materials having been tested and in view of the different test conditions and test rigs.

A point of discussion is the possibility of dissolution effects on oxide scales. We think that we have found in the literature sufficient indications for this effect warranting further investigation. This effect would then also affect the evolution of oxide scales under dynamic conditions. It may be rather important for low oxygen contents in the liquid metal.

Dissolution attack of austenitic steels at 550°C and higher is reported in the literature although the oxygen content in the lead-bismuth alloy should have been high enough for oxide scale formation. One explanation was thought to be the decrease of the oxygen activity with increasing temperature. We think that this might be due to mechanical effects debonding and spalling of the oxide scale at the locations affected by dissolution attack.

References

[1]   T. Malkow, H. Steiner, H. Muscher, J. Konys, Journ. Nucl. Mat. 335 (2004) 199

[2]   H. Steiner, J. Konys, Journ. Nucl. Mat. 348 (2006), 18-25

[3]   X. He, N. Li, M. Mineev, J. Nucl. Mater. 297 (2001) 214-219

[4]   J. Zhang, N. Li, J. Nucl. Mat. 321 (2003) 184-191

[5]   J. Zhang, N. Li, Corrosion 60 (2004) 331-341

[6]   J. Zhang, N. Li, J. Nucl. Mater. 326 (2004) 201-210

[7]   F. Balbaud-Celerier, F. Barbier, J. Nucl. Mater. 289 (2001) 227-242

[8]   E. Buckingham, Phys. Rev. 4 (1914) 345- 376

[9]   L.C. Burmeister: Convective Heat Transfer, John Wiley & Sons N.Y. (1982)

[10]   C. S. Tedmon, J. Electroch. Soc. 113 (1966) 766 – 768

[11]   S. Z. Beer, Liquid Metals, Marcel Dekker, Inc., N.Y. (1972) 38-40

[12]   A.M. Azad, O:m: Sreedharan, J.B. Gnanamoorthy, J. Nucl. Mat. 144 (1987) 94-104

[13]   F.N. Mazandarany and R.D. Pehlke, Met. Trans. 4 () 1973-2067

[14]   M.G. Barker, T. Sample, Fus. Eng. Des. 14 (1991) 219

[15]   F. P. Berger, K. Hau, Int. J. Heat Mass Transfer 20 (1977) 1185

[16]   D. C. Silverman, Corrosion 55 (1999) 1115

[17]   P. Harriott, R.M. Hamilton, Chem. Eng. Sci. 20 (1965) 1073

[18]   Verein Deutscher Ingenieure, VDI-Wärmeatlas Berechnungsblätter für den Wärmeübergang, 8. Auflage 1997, Springer-Verlag Berlin Heidelberg, Ga1-Gb5

[19]   B.F. Gromov, et al, Nucl. Eng. Des. 173 (1997) 207

[20]   A. Heinzel, FZKA 6823 (2003)

[21]   C. Schroer, Z. Voß, O. Wedemeyer, J. Novotny, J. Konys, A. Heinzel, A. Weisenburger, G. Müller, internal report (2005)

[22]   J. Zhang, N. Li, Y. Chen, A.E. Rusanov, J. Nucl. Mat. 336 (2005) 1-10

[23]   N. Li Journ. Nucl. Mat. 300 (2002) 73-81

[24]   I. Barin, Thermochemical Data of Pure Substances, VCH, Weinheim (1989)

[25]   G. Müller, G. Schumacher, F. Zimmermann, J. Nucl. Mat. 278 (2000) 85-95

[26]   V. Coen, T. Sample, Fus.Technol. Proceed. 16th SOFT, London (1990) 248-252

[27]   M.G. Barker, V. Coen, H. Kolbe, J. A. Lees, L. Orecchia, T. Sample, J. Nucl. Mat. 155-157 (1988) 732

[28]   H.U. Borgstedt, H.D. Röhrig, J. Nucl. Mater. 179-181 (1991) 596

[29]   H.U. Borgstedt, H. Feuerstein, J. Nucl. Mater. 191-194 (1992) 988-991

[30] H.U. Borgstedt, C. Guminski, J. Nucl. Mater. 303 (2002) 240-241

[31] H. Feuerstein, H. Gräbner, J. Oschinski, J. Beyer, S. Horn, L. Hörner, K. Santo, FZKA 5596 (1995)

[32] C. Guminski in H.U:Borgstedt Liquid Metal Systems Material Behavior and Physical Chemistry in Liquid Metal Systems 2, 345, Plenum Press, N.Y. (1995)

[33] Y. Kurata, M. Futakawa, K. Kikuchi, S. Saito, T. Osugi, J. Nucl. Mat. 301 (2002) 28-34

[34] S. Osgerby, Mat. High Temp. 17(2) (2000) 307-310

[35] L. Nieto Hierro, V. Rohr, P.J. Ennis, M. Schütze and W.J. Quadakkers, Mat. and Corr. 56 (2005) 890-896

[36] Zs. Tökei, H. Viefhaus, H.J. Grabke, Appl. Surf. Sci. 165 (2000) 23-33

[37] A.F. Smith, Corr. Sci. 22 (1982) 857-865

[38] M. Saito, H. Furuya and M. Sugisaki, J. Nucl. Mat. 135 (1985) 11-17

[39] H.E. Evans, Int. Mat. Rev. 40 (1995) 1-40

[40] C. Schroer, Z. Voss, O. Wedemeyer, J. Novotny and J. Konys, Interim Report (May 2004)

[41] G. Müller FZKA 6422 (2000)

[42] R. Dieckmann, H. Schmalried, Ber. Bunsen-Ges. 81 (1977) 344

[43] B.F. Gromov, Y.I. Orloy, P.N. Martynov, K. D. Ivanov, V. A. Gulevski, in H.U. Borgstedt, G. Frees (Eds), Liquid Metal Systems, Plenum Press, N.Y. (1995) 339

[44] V. Markov, Seminar on the concept of Lead-Cooled Fast Reactors, Cadarache (1997) unpublished

[45] H. Glasbrenner, J. Konys, G. Mueller, A. Rusanov, J. Nucl. Mat. 296 (2001) 237-242

[46] A. Terlaine, DEMETRA-Meeting, Paris, Oct. 2005

[47] C. Fazio, G. Benamati, C. Martini, G. Palombarini, J. Nucl. Mat. 296 (2001) 243-248

[48] F. Barbier, A. Rusanov, J. Nucl. Mat. 296 (2001) 231-236

[49] C. Schroer, Z. Voß, O. Wedemeyer, J. Novotny, J. Konys, A. Heinzel, A. Weisenburger, G. Müller, internal report

[50] C. Schroer, Z. Voss, O. Wedemeyer, J. Novotny and J. Konys, Int. Workshop on Spallation Mat. Techn. (2005) Thun

[51] G. Müller, G. Schumacher, A. Weisenburger, A. Heinzel, F. Zimmermann, T. Furukawa, K. Aoto, JNC TY9400 2002-023 (2002)

[52] G. Müller, G. Schumacher, A. Weisenburger, A. Heinzel, F. Zimmermann, T. Furukawa, K. Aoto, JNC TY9400 2003-026 (2002)

[53] G. Müller, G. Schumacher, A. Weisenburger, A. Heinzel, F. Zimmermann, T. Furukawa, K. Aoto, JNC TY9400 2003-028 (2002)

[54] G. Benamati, C. Fazio, H. Piankova, A. Rusanov, J. Nucl. Mat. 301 (2002) 23 – 37

[55] F. Balbaud-Celerier, P. Beloffre, A. Terlani, A. Rusanov, J. Phys. IV France 12 (2002) Pr8-177

[56] G. Müller, A. Heinzel, J. Konys, G. Schumacher, A. Weisenburger, F. Zimmermann, V. Engelko, A. Rusanov, V. Markov, J. Nucl. Mat. 301 (2002) 40-46

[57] L. Soler Crispo, F.J. Martin Munoz, D. Gomez Briceno, Journ. Nucl. Mat. 296 (2001) 273-281

[58] J.U. Knebel, X. Cheng, C.-H. Lefhalm, G. Müller, G. Schumacher, J. Konys, H. Glasbrenner, Nucl. Eng. Des. 202 (2000) 279

[59] J. Konys, W. Krauss, Z. Voss, O. Wedemeyer, J. Nucl. Mat. 329-333 (2004) 1379-1383

Notation

T = temperature

t = time

x = axial position

C = concentration

V, u = velocity

D = diffusivity

K = mass transfer coefficient

d= diameter

A = area

U = circumference

Re = Reynolds number

Sc = Schmidt number

Pr = Prandl number

Nu = Nusselt number

Sh = Sherwood number

R = gas constant

M = atomic weight

P = porosity

L = length

G = free energy of formation

p = pressure

a = activity

ν = kinematic viscosity

ρ = density

δ = layer thickness

λ = friction coefficient

τ = shear stress

Φ = Pilling-Bedworth ratio

Superscripts and subscripts

w = wall

b = bulk

hyd = hydraulic

fl = fluid

ch = channel

o = oxygen

ox = oxide

me = metal

m.tr. = magnetic trap

s.l. = surface layer

s = saturation or surface

la = laminar

turb = turbulent

ma = magnetite

sp = spinel